TAMPEREEN TEKNILLINEN YLIOPISTO
TAMPERE UNIVERSITY OF TECHNOLOGY

ANNIINA OJANPERÄ

MESOSCOPIC PEROVSKITE SOLAR CELLS: EFFICIENCY ENHANCEMENT VIA OPTIMIZATION OF THE TITANIA ANODE

Master of Science Thesis

Examiner: D. Sc. (Tech) Paola Vivo
Examiner and topic approved by the Faculty Council of the Faculty of Natural Sciences
on 4th November 2015

ABSTRACT

ANNIINA OJANPERÄ: MESOSCOPIC PEROVSKITE SOLAR CELLS: EFFICIENCY ENHANCEMENT VIA OPTIMIZATION OF THE TITANIA ANODE
Tampere University of technology
Master of Science Thesis, 53 pages
November 2015
Master's Degree Programme in Science and Engineering
Major: Chemistry
Examiner: D. Sc. (Tech) Paola Vivo

Keywords: perovskite, solar cell, titania, anode, compact layer, mesoporous layer

Perovskite solar cells have lately attracted a tremendous attention in the scientific community, due to an incredible boost in their conversion efficiency (from 9 to over 20 %) in the last three years. The development of perovskite solar cells has been extremely rapid, thus providing efficiency enhancements at a faster rate compared to that of any other solar cell technology.

The most common perovskite-based solar cell architecture is the mesoscopic perovskite solar cell. Its structure employs a compact layer and a mesoporous metal oxide layer as the cell anode. Typically, the anode consists of titania, which is an *n*-type semiconductor. The compact layer acts as a blocking layer by preventing the recombination of charges. The mesoporous layer extracts electrons from the excited perovskite upon light absorption, and transports them to the electrode.

The present Thesis studies the effect of titania anode modification on the power conversion efficiency of mesoscopic perovskite solar cells. The experiments carried out include the fabrication and the characterization of titania-based mesoscopic solar cells. The research methods used in this work are scanning electron microscopy, steady-state absorption and reflectance spectroscopies, and *I-V* measurements.

The titania anode, i.e. the compact and mesoporous layer, was optimized as the result of the study. The best solution to produce compact titania layer by spin-coating was found. It was observed that the mesoscopic perovskites solar cells with highest efficiency had a thin mesoporous titania layer. Among the tested thicknesses, 190 nm was the optimal value for the mesoporous layer thickness, leading to the best cell performance. The highest achieved efficiency of the solar cells prepared in this work was 9.55 %.

TIIVISTELMÄ

ANNIINA OJANPERÄ: MESOSKOOPPISET PEROVSKIITTI-AURINKOKENNOT: HYÖTYSUHTEEN PARANTAMINEN TITAANIDIOKSIDIANODIN OPTIMOINNILLA
Tampereen teknillinen yliopisto
Diplomityö, 53 sivua
Marraskuu 2015
Teknis-luonnontieteellinen diplomi-insinöörin tutkinto-ohjelma
Pääaine: Kemia
Tarkastaja: tutkijatohtori, D. Sc. Paola Vivo

Avainsanat: perovskiitti, aurinkokenno, titaanidioksidi, anodi, kompakti kerros, mesohuokoinen kerros

Perovskiitti –aurinkokennot ovat saavuttaneet laaja-alaista huomiota aurinkokenno-tutkimuksen alalla. Niiden hyötysuhde on ylittänyt 20 %, mikä tekee perovskiitista varteenotettavan vaihtoehdon aurinkokennoissa käytettäväksi valoa absorboivaksi materiaaliksi. Perovskiitti –aurinkokennojen kehitys on ollut nopeaa ja niiden hyötysuhteet ovat nousseet räjähdysmäisesti verrattuna muihin aurinkokennotyyppeihin.

Yleisin perovskiitti –aurinkokennoissa käytetty anodi koostuu kompaktista mesohuokoisesta metallioksidista. Tällaisia kennoja kutsutaan mesoskooppisiksi perovskiitti -aurinkokennoiksi. Tyypillisin anodimateriaali on *n*-tyypin puolijohde, titaanidioksidi. Kompakti kerros estää varausten rekombinaation. Mesohuokoinen kerros eristää elektronit valolla viritetystä perovskiitista ja kuljettaa ne elektrodille.

Tämä diplomityö tutkii titaanidioksidi –anodin muokkauksen vaikutusta mesoskooppisten perovskiitti –aurinkokennojen hyötysuhteisiin. Kokeellinen tutkimus käsitti mesoskooppisten aurinkokennojen valmistuksen ja niiden karakterisoinnin. Tutkimusmetodeina käytettiin pyyhkäisyelektronimikroskopiaa, vakiotilan absorptio- ja reflektanssispektroskopiaa ja *I-V* mittauksia.

Tutkimuksessa optimoitiin kompaktin titaanidioksidi -anodin rakennetta muun muassa löytämällä spin-päällystysmenetelmään parhaiten soveltuva liuoskoostumus. Mesoskooppisten perovskiitti –aurinkokennojen hyötysuhteen havaittiin parantuvan, kun niissä käytettiin mahdollisimman ohutta titaanidioksidikerrosta. Parhaimmaksi osoittautui 190 nm paksu mesohuokoinen kerros. Korkein diplomityössä saavutettu aurinkokennon hyötysuhde on 9,55 %.

PREFACE

This work has been carried out in the Chemistry Laboratory at the Department of Chemistry and Bioengineering, Tampere University of Technology. First of all I would like to thank *emeritus professor* Helge Lemmetyinen, who has embraced me as a member of the Supramolecular Photochemistry Research Group and provided me all opportunities to make this Thesis including his co-supervision and careful examination of the Thesis. Especially I would like to thank the nominated examiner and the co-supervisor Dr. Paola Vivo for guiding and supporting me during the process.

I am grateful to Dr. Antonio Abate and his research group in Adolphe Merkle Institute in Fribourg, Switzerland. He and Ph.D. students M. Sc. Bart Roose and M. Sc. Sandy Sanchez Alonso gave me valuable knowledge and an unforgettable chance to visit a research laboratory abroad. I would also like to thank Dr. Hashmi Ghufran Syed from Aalto University, and Ph.D. student M. Sc. Muhammad Talha Masood and B. Sc. Pontus Wistbacka from Åbo Akademi for their help and advice.

I would like to thank all the members of Supramolecular Photochemistry Research Group for guidance and helping me with all my issues during this work. I want to express my gratitude to M. Sc. Tero-Petri Ruoko and summer trainees Pierre Degot and Thomas Mokus for their great company both at work and in free time. Special thanks go to M. Sc. Arto Hiltunen for his irreplaceable support and friendship.

To all my friends, who I have met at TUT over the years, I am also thankful for providing counterbalance for studies and this Thesis work. I also want to thank my dearest home town friends for being there for me whenever needed.

Finally, I would like to express my gratitude to my parents and my sisters whose support I can always count on.

Tampere, 24.11.2015

Anniina Ojanperä

CONTENTS

1. INTRODUCTION 1
2. THEORETICAL BACKGROUND 3
2.1 Electronic state transitions and charge transfer 3
2.1.1 Absorption and scattering 3
2.1.2 Electronic state transitions 4
2.1.3 Electron transfer 5
2.2 Perovskite 6
2.2.1 Structure and properties 6
2.2.2 Stability 7
2.3 Perovskite solar cells and their development 9
2.4 Solar cell generations 9
2.4.1 Hybrid solar cells 10
2.4.2 Solid-state dye-sensitized solar cells 11
2.4.3 Perovskite solar cells 12
2.5 Components of mesoscopic perovskite solar cells 14
2.5.1 Compact metal oxide layer 14
2.5.2 Mesoporous metal oxide layer 14
2.5.3 Hole transport layer 16
2.5.4 Counter electrode 18
2.6 Characterization and evaluation of solar cells 18
2.6.1 Measuring perovskite solar cell performance 21
3. MATERIALS AND METHODS 23
3.1 Sample preparation 23
3.1.1 Materials and solution preparations 24
3.1.2 Spin-coating 25
3.1.3 Sequential deposition of perovskite 26
3.1.4 Thermal evaporation 27
3.2 Research methods 28
3.2.1 Scanning electron microscopy 28
3.2.2 Steady-state absorbance and reflectance measurements 28
3.2.3 *I-V* measurements 29
4. RESULTS AND DISCUSSION 31
4.1 Optimization of compact titania layer 31
4.2 Optimization of mesoporous titania layer 36
4.3 Characterization of perovskite and hole transport layer 42
5. CONCLUSIONS 47
REFERENCES 49

LIST OF SYMBOLS AND ABBREVIATIONS

AM	air mass
DSSC	dye-sensitized solar cell
ETM	electron transport material
EtOH	ethanol
FK 102	tris(2-(1*H*-pyrazol-1-yl)pyridine)cobalt(III) PF6 salt
FTO	fluorine tin oxide
IPA	2-propanol/isopropanol
ITO	indium tin oxide
HOMO	highest unoccupied molecular orbital
HTM/HTL	hole transport material/layer
LUMO	lowest unoccupied molecular orbital
LiTFSI	bis(trifluoro-methane)sulfonimide lithium salt
MAI	methyl ammonium iodide
$MAPbI_2$	methyl ammonium lead iodide
SEM	scanning electron microscopy
spiro-OMeTAD	2,2',7,7'-tetrakis-(N,N-di-4-methoxy-phenylamino)-9,9'-spirobifluorene
ssDSSC	solid-state dye-sensitized solar cell
tBP	tert-butyl pyridine
TCO	transparent conducting oxide

λ	wavelength
A	absorbance
A_{cell}	irradiated area of the solar cell
ε	molar absorption coefficient
$e\Phi$	photon flux
E	energy
FF	fill factor
h	Planck's constant
I_λ	light intensity at wavelength λ
I-V	current-voltage
IPCE	incident photon-to-current conversion efficiency
I_{SC}	short circuit current
J-V	current density-voltage
J_{SC}	short circuit current density
l	length
η	energy conversion efficiency
P_{in}	irradiance of the incident light to the surface
P_{max}	maximum power point
R	reflectance
T	transmittance
v	frequency
V_{OC}	open circuit voltage
φ	angle of elevation of the Sun

1. INTRODUCTION

The Sun emits ultraviolet, visible, and infrared radiation. The word light is used normally to indicate the portion of the electromagnetic radiation spectrum that is visible to the human eye. Visible light corresponds to the wavelength range from 390 to 750 nm, lying between the ultraviolet and infrared wavelengths (Figure 1) [1, 2].

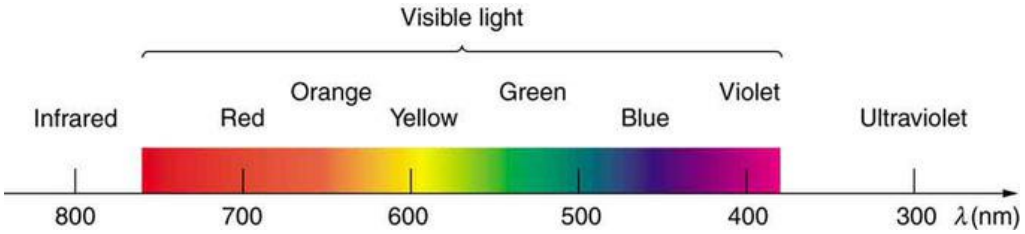

Figure 1. *Visible light spectrum [1].*

The energy of the Sun reaches the earth's surface with power 1.7×10^5 TW. It is estimated that 600 TW of the solar energy could be harnessed [2]. In 2012 the world energy consumption was 8 979 Mtoe, which corresponds to 104 400 TWh or 12 TW [3]. The terrestrial solar energy is remarkably higher. Moreover, sunlight is free, unlimited, readily available, clean, and ubiquitous. This makes the solar energy one of the most attractive technologies to meet the energy needs.

The first solar cell, constructed in 1954, was based on silicon. Silicon solar cells belong to the first generation of solar cells. To date, their record efficiency is 25.6 % [4, 5]. Perovskite-based solar cells have gained a tremendous momentum in photovoltaics research over the past few years [6]. In 2006, the first perovskites-based solar cells were fabricated, resulting in modest efficiency of 2.2 %. Their breakthrough took place in 2012 as efficiency of nearly 10 % was achieved [7]. Editors of *Science* and *Nature* chose perovskite solar cell technology as one of the biggest scientific breakthroughs of 2013. To date, the record certified efficiency of perovskite solar cells is 20.1 % [5, 7]. Silicon solar cells have been developed for more than 60 years. Nevertheless, perovskite solar cells are becoming as efficient as their first-generation silicon-based cells, even though they have been researched for less than a decade.

Although perovskite is one of the most important light absorbing materials in solar cells, its employment has some issues. The best-performing solar cells contain lead, which is toxic. Perovskite suffers also from degradation mainly due to moisture and UV light [7-9]. The perovskite solar cell research has been extensive only for a few years.

As the research on this technology will continue further, it is expected that the stability issues will be overcome.

The perovskite solar cells were first incorporated on mesoporous titania in solid-state dye-sensitized solar cells. In addition to this mesoscopic structure, an alternative perovskite solar cell configuration has been proposed, namely the so-called planar heterojunction.

This work focuses on mesoscopic perovskite solar cells [7, 9]. More specifically, it demonstrates how to improve the efficiency of perovskite solar cells by optimizing the titania anode. Special attention was paid to the measurements method, in order to minimize overestimations.

The present Thesis is organized as follows. Section 2 introduces the theoretical background of perovskite solar cells. Experiments together with their results and analysis are discussed in Sections 3 and 4. Section 5 summarizes the main findings and outlines the key directions for future research stemming from them.

2. THEORETICAL BACKGROUND

This section introduces the theory behind perovskite solar cells and their operation. First, the electronic state transitions and charge transfer are discussed, followed by a description of perovskite and its properties. The development of solar cells from the first generation solar cells to perovskite solar cells is then described, together with their operation. Finally, the main techniques for the evaluation and the characterization of solar cells are presented.

2.1 Electronic state transitions and charge transfer

The operation of a solar cell combines absorption of light, which is a transition between electronic states of the absorbing compound, with effective charge separation and transfer. This sub-section discusses the interaction between light and matter. The most important electronic state transitions and charge transfer mechanisms for the solar cell operation are introduced.

2.1.1 Absorption and scattering

An atom or a molecule interacts with incident light either by scattering or by absorbing the light depending on the energy of a photon.

Scattering is the deflection of a unidirectional beam of light from its original direction in several paths. Reflection is the process by which electromagnetic radiation is returned either at the boundary between two media (surface reflection) or at the interior of medium (volume reflection). Scattering can be associated with reflection and transmission [10, 11].

Regular or specular reflection is reflection with no associated scattering, whereas diffuse reflection represents the combination of both reflection and scattering. The electromagnetic radiation passing through a medium is called transmission. Transmission is called regular or direct if no scattering takes place. Regular reflection and transmission of a unidirectional beam result in another unidirectional beam [11].

The energy of irradiation E is dependent on its frequency, ν

$$E = h\nu, \tag{1}$$

where h is Planck's constant [12]. Absorption is a process, by which a molecule (M) becomes excited (M*) when an electron from an orbital of the molecule in the ground state is promoted to an unoccupied orbital of higher energy by the absorption of a photon

$$\mathrm{M} + h\nu \rightarrow \mathrm{M}^{*}. \tag{2}$$

Transmittance, T, is a measure of the transmitted light intensity in relation to the incident light. Similarly, reflectance, R, is the ratio of the reflected radiant power to the incident radiant power. Absorbance, A, is used to describe the efficiency of the light absorption by an absorbing medium. Absorbance at a wavelength (λ), A_λ, is defined as

$$A_\lambda = \log \frac{I_\lambda^0}{I_\lambda} = -\log T(\lambda), \tag{3}$$

where I_λ^0 and I_λ are the light intensities of the beams entering and leaving the absorbing medium, respectively. Absorbance can be expressed also as the Beer-Lambert law

$$A_\lambda = \varepsilon(\lambda) l, \tag{4}$$

where ε is the molar absorption coefficient (L $\mathrm{mol^{-1}}$ $\mathrm{cm^{-1}}$), c is the concentration (mol $\mathrm{L^{-1}}$), and l represents the thickness of the absorbing medium (cm) [11, 13]. Absorption promotes an electron form the highest occupied molecular orbital to the lowest or higher unoccupied molecular orbital in a molecule [12].

2.1.2 Electronic state transitions

In addition to absorption, there are several possible transitions occurring between the electronic states. The Jablonski diagram (Figure 2) visualizes the electronic states of a molecule and the possible light-induced transitions between the states. S_0 denotes the singlet state. S_1 and S_2 refer to the excited states of the same multiplicity. Correspondingly, T refers to the triplet states [14]. Absorption, fluorescence, and internal conversion are singlet-singlet transitions, but the latest can also be a triplet-triplet transition. Inter-system crossing is a process, in which the singlet state undergoes to the triplet excited state, or opposite. A radiative transition from the triplet state T_1 to the ground state S_0 is an inter-system crossing process as well, but is called phosphorescence. Fluorescence is the spontaneous emission of radiation accompanying the relaxation from the excited molecular entity with retention of spin multiplicity, most often from the lowest excited singlet state to the singlet ground state, $S_1 \rightarrow S_0$ [13].

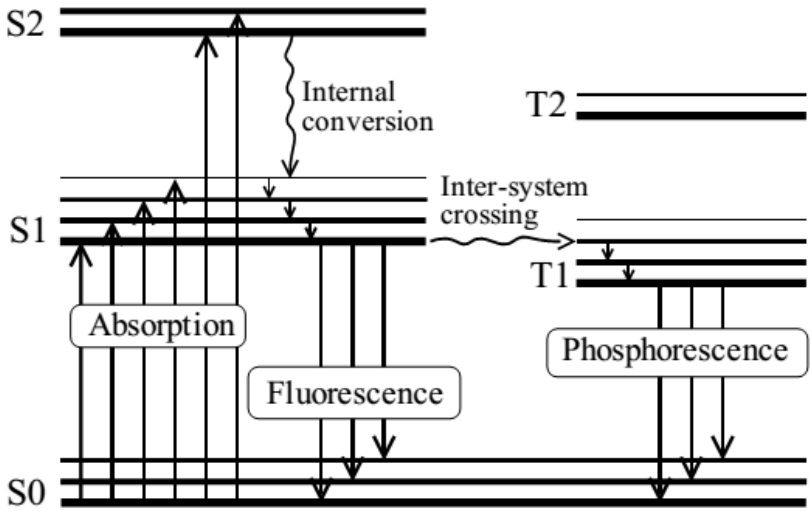

Figure 2. *Jablonski diagram [14].*

Excited molecules stay in the S_1 state for a certain time prior to the de-excitation processes, namely internal conversion, inter-system crossing, and fluorescence. Internal conversion and inter-system crossing are non-radiative transitions. Inter-system crossing is a forbidden transition because it changes the multiplicity. For this reason it is very slow compared to other de-excitation processes [12, 13].

2.1.3 Electron transfer

In addition to the spontaneous deactivation processes described in the previous chapter, the excited state can be quenched via several intermolecular processes, such as electron transfer, excimer and exciplex formation, and energy transfer. Most de-excitation processes involve an excited molecule (M*) and a quencher molecule (Q). The electron transfer occurs between two molecules, donor (D) and acceptor (A). It can be either an oxidative or a reductive reaction, as presented in Figure 3.

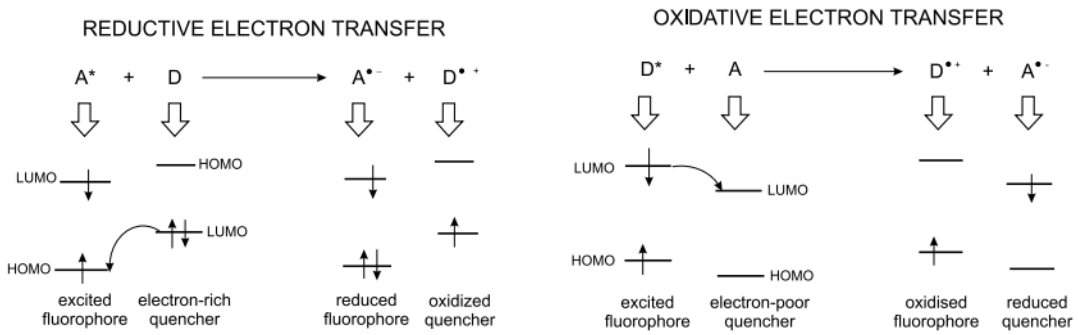

Figure 3. *Reductive and oxidative electron transfer [13].*

The photoinduced electron transfer takes place in many photochemical reactions. It is an important process in the photosynthesis. The operation of a solar cell requires electron

transfer after the photoactive moiety of the solar cell is excited by the photon absorption [13].

2.2 Perovskite

Perovskite was first discovered by Gustav Rose in 1839, with the identification of the calcium titanate ($CaTiO_3$) compound. Perovskites, i.e. any material having same crystal structure as $CaTiO_3$, are named after the Russian mineralogist L.A. Perovski, who first characterized them. Perovskites can be deposited in solar cells via solution- or vapor-based methods [7, 15].

2.2.1 Structure and properties

The ideal structure of pure perovskite compound is a network consisting of building blocks with an AMX_3 structure, where M and X represent a metal cation and an oxide (or halide) anion, respectively. Together they form an octahedral MX_6 arrangement, where M is in the center of the octahedron and X are in the corners. A denotes a large metal cation, which is centered in the hole formed by eight MX_6 octahedra. The basic structure of perovskites is presented in Figure 4. In organic-inorganic hybrid perovskites A is an organic cation [15].

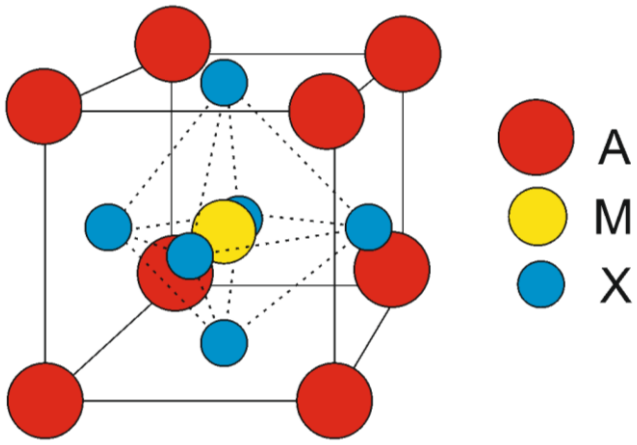

Figure 4. *Crystal structure of perovskite.*

Pure perovskite compound has a cubic geometry, but in nature it exits as pseudo-cubic or distorted cubic. The distortions influence the physical properties of perovskites, such as the electronic and optical properties [15].

The perovskites, which are employed in solar cells, are mainly either single halide or mixed halide perovskites. Typical single halide perovskites are methylammonium lead iodide ($CH_3NH_3PbI_3$ or $MAPbI_3$, MA = $CH_3NH_3^+$) and methylammonium lead bromide ($CH_3NH_3PbBr_3$ or $MAPbBr_3$). A typical mixed halide perovskite structure for solar cells is $MAPbI_{3-x}Cl_x$, $MAPbI_{3-x}Br_x$ or $MAPbBr_{3-x}Cl_x$. In this work $MAPbI_3$ is used [7].

The charge transport properties of perovskites are ambipolar, which means that they exhibit both *p*-type and *n*-type behavior. This allows using perovskites in different solar cells configurations, as discussed in Section 2.4.3 [8, 16].

Hybrid perovskites have several properties, which favor their use in solar cell applications. They have high molar absorption coefficients and an outstanding light-harvesting performance over visible light range. For example, the molar extinction coefficient of $MAPbI_3$ is around 1.5×10^5 L mol^{-1} cm^{-1} at 550 nm, which is 2–3 times higher than organic dyes used in solid-state dye sensitized solar cells [8, 16].

Perovskites have large exciton diffusion lengths. The diffusion length in $MAPbI_3$ is around 130 nm for electrons and 110 nm for holes. In solar cells with a mesoporous structure the diffusion length is preferred to be shorter than the light absorption depth (500–600 nm). For devices with a planar junction configuration the situation is opposite [8, 16].

In addition, organolead halide perovskite-based solar cells have an ultra-fast charge generation, high carrier mobilities, balanced charge carrier mobilities, and slow recombination rates. For example perovskites have a 3–4 times higher mobility than titania [16]. Perovskites also have low exciton binding energies [17]. The band-level characteristics of perovskites are also suitable for solar cells [8]. The band gap of $MAPbI_3$ is 1.55 eV. Theoretically a semiconductor with a band gap of 1.5 eV can achieve a photocurrent as high as 27 mA/cm^2 [18].

The morphology and crystal structure play a key-role in achieving high efficiency perovskite solar cells [7]. Perovskites form either polycrystalline or single-crystalline structures depending on processing. Crystalline shape, grain sizes, and surface area have all an effect on charge recombination, transport, and photovoltaic performance. The polycrystalline perovskite has two main types of defects: point defects, which affect the *n*- or *p*-type characteristics, and grain boundaries acting as trap states or recombination centers [17].

If $MAPbI_3$ is formed via a sequential deposition method (see Section 3.1.3), it probably generates cuboid polycrystals. Unlike the polycrystalline thin films, the $MAPbI_3$ single-crystals have sharp band-edge absorption. Single crystals have low trap-state densities, which allow crystal growth with higher long-range structural ordering and thus improve carrier mobility [17].

2.2.2 Stability

Despite the remarkable potentials of perovskites, there are also some drawbacks. Lead has been utilized in the best performing perovskite cells. Lead is, however, toxic, which raises some concerning issues during the device fabrication, deployment, and disposal.

For this reason the European Union and some countries have restricted the use of lead in electronic devices. Perovskites also tend to degrade when exposed to moisture and ultraviolet radiation [8, 9]. In addition, temperature and solution processing affect the degradation significantly. The degradation is an obstacle for the reproducibility and long lifetime of perovskite solar cells [19].

Perovskite undergoes different chemical reactions upon varying laboratory conditions. Depending on the environmental conditions, the perovskite used in this work, $MAPbI_3$, is in an equilibrium with its components according to the following reaction

$$PbI_2 + CH_3NH_3I \rightleftharpoons CH_3NH_3PbI_3. \tag{5}$$

Lead iodide and methyl ammonium iodide may react with other components, which drive the equilibrium towards the starting materials. Perovskite can also degrade to other compounds under certain conditions [19].

Moisture and oxygen can influence the stability of the components of the equilibrium equation (1). If there is moisture, perovskite hydrolyzes and degrades as follows

$$\begin{aligned} &CH_3NH_3PbI_3\,(s) \rightleftharpoons PbI_2\,(s) + CH_3NH_3I\,(aq)\\ &CH_3NH_3I\,(aq) \rightleftharpoons CH_3NH_2\,(aq) + HI\,(aq)\\ &4\,HI\,(aq) + O_2\,(g) \rightleftharpoons 2\,I_2\,(aq) + 2\,H_2O\,(l)\\ &2\,HI\,(aq) \rightleftharpoons H_2\,(g) + I_2\,(s). \end{aligned} \tag{6}$$

The last of these reactions occurs under UV radiation. Due to the sensitivity to moisture and oxygen, perovskite fabrication is preferred to be carried out in a glove box filled with inert gases [19]. The degradation of perovskite in the presence of water is fast and the degradation is completed in several minutes [20].

Titania, TiO_2, is the most common photoanode material in perovskite solar cells. The presence of TiO_2, acting as catalyst for water oxidation, induces the degradation of perovskite under UV-light. In fact, titania extracts electrons from the perovskite compound's iodine ion I^-. Encapsulation of perovskite solar cells protects them from moisture. However, it is reported that, if titania anode is employed, encapsulation of perovskite solar attenuates their stability as they are exposed to UV light. This may be due to oxygen vacancies of titania [16, 19].

There are several sources in solutions, which may decompose perovskite. The crystal structure may be destroyed by components of solvents, solutes, additives, and impurities. For example, the commonly used additives for the hole transport material, such as 4-tert-butyl pyridine and bis(trifluoro-methane)sulfonimide lithium salts, might corrode perovskite due to them being dissolved in acetonitrile [19].

It is necessary to anneal perovskite films during their fabrication for formation of perovskite crystals [19]. Nevertheless, an excessive heating (above 120 °C) causes perovskite decomposition into its starting materials. If the temperature is still increased up to 300 °C, perovskite can degrade to PbI_2, CH_3NH_2, and HI [20].

2.3 Perovskite solar cells and their development

This Section introduces the concept of perovskite solar cells and the background for their development. Perovskite solar cells, employing both organic and inorganic materials, are categorized as hybrid solar cells. They belong to the third solar cell generation, and their development arises from the dye-sensitized solar cells. This Section introduces briefly the solar cell generations. Hybrid, dye-sensitized, and perovskite solar cells are discussed in detail and their function principles presented.

2.4 Solar cell generations

The first generation solar cells are based on crystalline and polycrystalline silicon. The first practical silicon solar cell with a 6 % efficiency was prepared in 1954. Silicon-based solar cells are still dominating the solar cell market. The highest efficiency for silicon-based solar cell is 25.6 %. Shortcomings of this generation solar cells are their high production cost, large energy consumption, and pollution during the fabrication [4, 5, 21].

The second generation thin film solar cells employ II-VI semiconductors, copper indium gallium selenide, cadmium telluride, and amorphous silicon. At best their efficiency is 21 %. The aim of the second generation solar cells was to reduce the high costs of the first generation solar cells by using thin film technology. The goal was to save bulk material costs. The performance of the second generation solar cells is slightly reduced compared to the first generation cells [5, 21, 22].

The third generation of solar cells were developed to reach high efficiencies with low costs [22]. It involves organic photovoltaics and organic-inorganic hybrid solar cells amongst others. Perovskite solar cells belong to this generation [18, 21]. Organic materials, having both conducting and semiconductor properties, represent a potential option for photovoltaics. Organic photovoltaics have the advantages of being cheap and simple to construct, and they have a high throughput manufacturing. Additionally, organic semiconductors have high absorption coefficients. Organic-inorganic hybrid solar cells combine both organic and inorganic semiconductors, aiming to benefit of the advantages of inorganic semiconductor materials and still be inexpensive to process [23].

The third generation solar cells have not yet achieved as high efficiencies and long lifetimes as the first and second generation solar cells. Nevertheless, they have several

advantages such as low fabrication cost, flexibility, and light weight, which make them tempting for photovoltaic applications [21].

2.4.1 Hybrid solar cells

Hybrid solar cells combine organic with inorganic materials, aiming to utilize the advantages of both material groups. Compared to organic materials, the inorganic ones provide better stability, higher carrier mobility, and more flexibility to arrange them into different nanostructures. The hybrid solar cells have also the advantages of organic materials such as their light absorption properties and simple solution processability [21, 23].

Organic solar cells can be represented, at very high level, by two electrodes with different work functions, interleaved by a photoactive layer located between the electrodes. In traditional organic solar cells, the photoactive layer consists of organic donor and organic acceptor materials. In hybrid solar cells, the electron acceptor is replaced with an inorganic material. Inorganic semiconductors together with organic semiconductors form a *p-n* junction. They can form a single interface in a bilayer heterojunction structure or a dispersed interface in a bulk heterojunction structure [21, 23, 24]. These structures are shown in Figure 5.

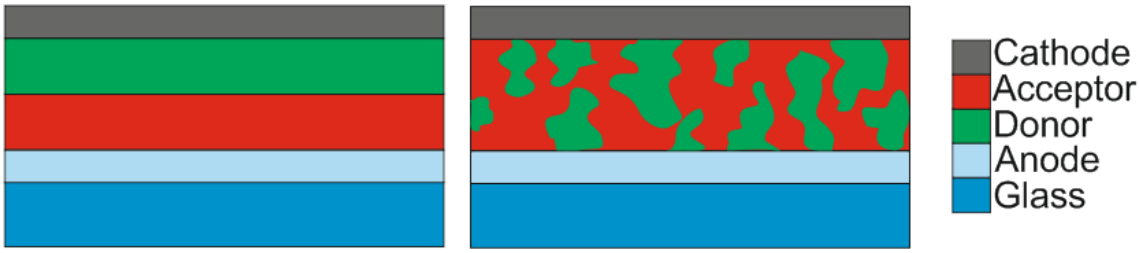

Figure 5. *Structure of bilayer heterojunction (left) and bulk heterojunction hybrid solar cells.*

The inorganic acceptor materials have many advantages over the organic acceptor ones. One of the major disadvantages of the organic acceptors is that they are prone to photodegradation. The operation of hybrid polymer solar cells requires that excitons dissociate due to the suitable HOMO level energy of the donor and the valence band edge of the acceptor. The donor material absorbs a photon, which results in an exciton formation. In the hybrid solar cells excitons dissociate into electrons and holes at the donor-acceptor interface. Electrons travel through the acceptor material to be finally collected at the cathode. Holes move across the donor material towards the anode [21, 23].

2.4.2 Solid-state dye-sensitized solar cells

Perovskite solar cells stemmed from the dye-sensitized solar cells (DSSC), which were invented in 1991 by O'Regan and Grätzel as they constructed a solar cell, in which they deposited nanocrystalline titania film coated with a molecular dye [25]. The dye-sensitized solar cells were thought to be a potential alternative to the conventional inorganic silicon-based solar cells, since their processing costs are low and materials inexpensive. Nevertheless, the dye-sensitized solar cells suffer from leakage problems, due to the presence of a liquid electrolyte. In 1998 the liquid electrolyte was for the first time replaced with a solid hole transporting material in the so-called solid-state dye-sensitized solar cells (ssDSSC) [7].

Dye-sensitized solar cells typically employ nanostructured titania as an electron conductor on top of a transparent conducting oxide (TCO) material on glass or plastic substrate. The electron conductor can be also some other metal oxide, such as zinc oxide or tin dioxide. The light absorbing dye lies on top of the electron conductor material. The next layer is a liquid redox electrolyte for the dye regeneration. For ssDSSCs the liquid electrolyte is replaced with the solid hole transport material (HTM). The top layer is a counter electrode to collect electrons. In ssDSSCs there is a thin compact layer between the mesoporous layer and TCO material to prevent any direct contact between TCO and HTM. Titania is typically employed as the compact layer material [2, 15]. The structure of the solid-state dye-sensitized solar cell is presented in Figure 6.

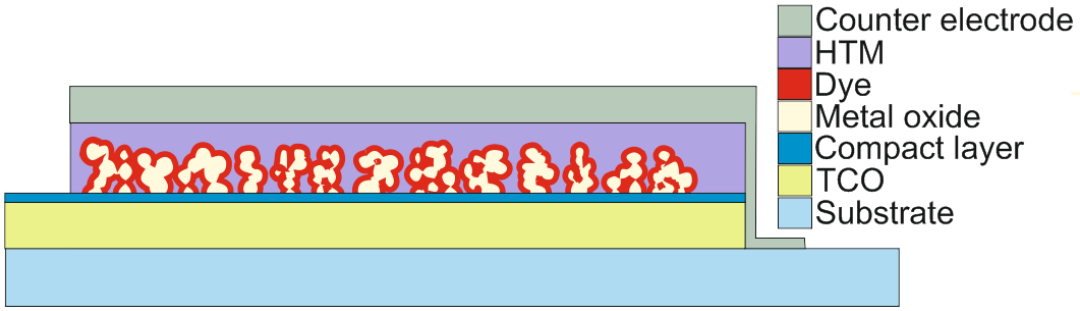

Figure 6. *Structure of ssDSSC.*

The function of a DSSC differs from that of a *p-n* junction based solar cell. The inspiration behind the working principle is taken from the photosynthesis. Photons excite the dye molecules under light absorption. Charges separate at the interface between the electron and hole conducting materials. Electrons are injected into the conduction band of the inorganic semiconductor, and they migrate to the working electrode. The oxidized dye is regenerated by electron transfer from the donor species of the redox medium. Holes migrate to the counter electrode. The donor is reduced and the excited state of the dye decays. Injected electrons recombine with the acceptor in the redox medium [26].

It has been predicted that the solid-state dye-sensitized solar cells could achieve efficiencies over 20 %. Despite extensive research, the efficiencies have not reached the theoretical limit as the record efficiency is 11.9 % [5, 26].

2.4.3 Perovskite solar cells

Perovskites were incorporated for the first time into dye-sensititized solar cells in 2006 by Miyasaka *et al.* They reported cells with $CH_3NH_3PbBr_3$ perovskite on mesoporous TiO_2 anodes having efficiency of 2.2 %. Later in 2009, after replacing bromine with iodine, the efficiency was only increased up to 3.8 %. Moreover, their cells had stability issues because of the liquid electrolyte [9, 18].

A breakthrough for perovskites in solar cell took place in 2012 as Grätzel *et al.* and almost simultaneously Snaith *et al.* reached 9.7 % and 7.6 % efficiencies, respectively, by using perovskites as light harvesters in solid-state dye-sensitized solar cells [7]. Since then, perovskite solar cells have gained a tremendous interest in the research community, and their development has been extremely fast. The efficiencies have improved rapidly as different structures and fabrication methods have been studied [18]. To date, the efficiency of perovskite solar cells has exceeded 20 % as the record certified efficiency is 20.1 % [5].

Perovskite solar cells can be divided into three groups according to their device architecture: mesoscopic perovskite solar cells, meso-superstructured perovskite solar cells, and planar heterojunction perovskite solar cells. The configuration of the planar heterojunction solar cells can be either positive or inverted [7, 20]. This will be explained later. The mesoscopic and planar heterojunction structures are depicted in Figure 7.

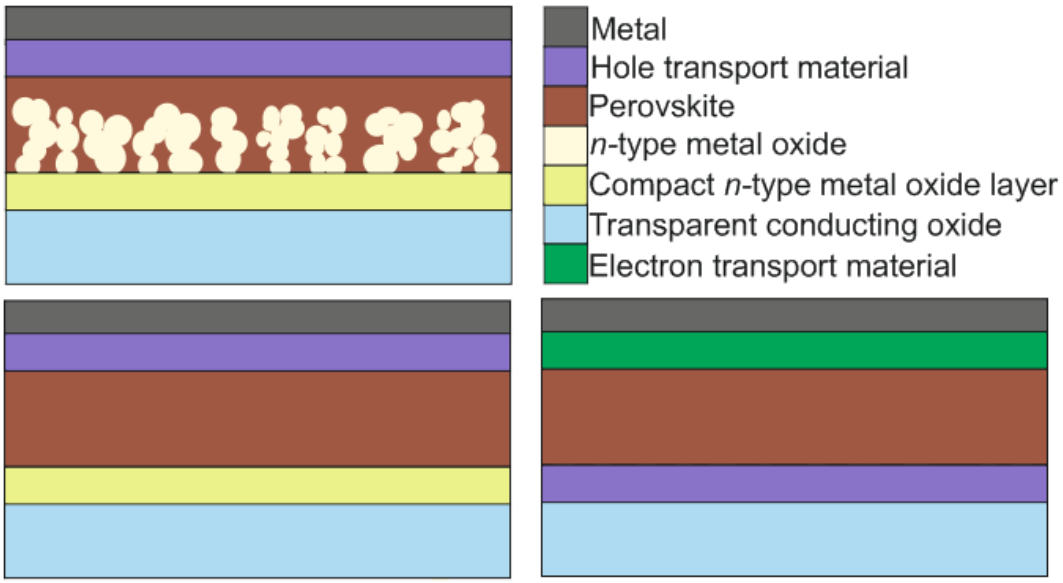

Figure 7. *Perovskite solar cell structures: a mesoscopic (top), a planar heterojunction (bottom left), and an inverted perovskite (bottom right) solar cell.*

The mesoscopic perovskite solar cells or so-called perovskite-sensitized mesoporous cells have a similar structure to the solid-state dye-sensitized solar cells. Typically perovskite is used as light absorber on top of the titania network, and forms there a capping layer. On top of perovskite there are a hole transport material (HTM) layer and a counter electrode [7, 15, 20]. This work focuses on the mesoscopic perovskite solar cells.

The functional principles of the mesoscopic perovskite solar cells are the same as for DSSCs. The desired processes include photoexcitation in perovskite and electron and hole transfers. There are also undesired processes such as recombination of photogenerated species and back charge transfer at interfaces. For high performance perovskite solar cells, as for all solar cells, the undesired processes should be much slower than the desired processes [7, 20].

The structure of meso-superstuctured perovskite solar cells is similar to the mesoscopic structure. Compared to the mesoscopic cells the mesoporous *n*-type conducting metal oxide is replaced with a porous insulating metal oxide layer. The insulating metal oxide is deposited on top of compact *n*-type conducting metal oxide [16]. The insulating metal oxide works only as a scaffold. In this configuration, perovskite acts as an intrinsic absorber and electron transport material (ETM) [7].

The planar heterojunction perovskite solar cells do not employ porous metal oxides. In them perovskite is between the hole transport and the electron transport layers and acts as an ambipolar layer in the *p*-*i*-*n* junction. In case of positive configuration the electron transport layer is on top of the TCO substrate. On the top of the electron transport layer there are perovskite, hole transport layer, and counter electrode. The inverted structure

stems from the bulk heterojunction solar cells: the TCO substrate is coated with *p*-type material followed by a perovskite layer, *n*-type layer, and finally the anode [7, 27].

2.5 Components of mesoscopic perovskite solar cells

This Section introduces the components of the mesoscopic perovskite solar cells. They employ an *n*-type semiconducting mesoporous layer, which is in most cases prepared from titania. The mesoscopic cell is constructed on a conductive fluorine doped tin oxide (FTO) coated glass substrate. FTO is coated with a compact layer, on top of which the mesoporous layer is built, followed by a perovskite layer and organic or inorganic hole transport material. The metal top-electrode completes the perovskite solar cell structure [7, 28]. FTO, together with the *n*-type semiconductor layer, forms the anode, while the metal layer together on HTM is the cathode of the mesoscopic solar cells [29].

2.5.1 Compact metal oxide layer

The compact layer is an essential part of the mesoscopic perovskite solar cells. It prevents a direct contact between the HTM and the FTO layers, which would create a short circuit in the cell. In addition, it prevents the holes generated in the perovskite layer or HTM layers from reaching the FTO anode, which would contribute negatively to the net current that can be extracted from the cell because the holes should be collected at the cathode. Since the compact layer guides the electrons and holes to their respective electrodes, it decreases the risk of the recombination of the charge carriers. As the contact area between the FTO layer and the perovskite or HTM layers is reduced, also the recombination is reduced. Pinholes in the compact layer would decrease the solar cell efficiency by allowing a contact between the materials. The most common compact layer material is titania [30, 31].

There are several methods to deposit titania compact layer, such as spin-coating from a precursor solution, spray-pyrolysis, and atomic layer deposition [7]. The compact layer is deposited on transparent conducting oxide (TCO) substrate. TCO is normally FTO, since it adheres well to titania. The compact layer should be as thin as possible, because a larger layer implies higher resistance, and thus lower fill factor and charge collection [29].

2.5.2 Mesoporous metal oxide layer

Inorganic semiconductor materials can be used to produce different and complex nanostructures. Titania is employed extensively in photovoltaic devices because of its desired properties. It is non-toxic, it has high chemical stability, low cost, strong photocatalytic activity, and high photoelectric conversion efficiency [21].

Mesoscopic perovskite solar cells employ an *n*-type mesoporous semiconducting layer. To inject excited electrons from perovskite to the mesoporous layer, the oxide layer should have lower conduction band than the excited state of perovskite. The *n*-type mesoporous material consists typically of titania nanoparticles [28, 29]. Titania extracts electrons which have been generated in perovskite. It also enhances the perovskite crystal transformation when sequential deposition method is used (see Section 3.1.3). Mesoporous titania layers can be fabricated by spin-coating, screen-printing, and doctor-blading [7].

Titania has three natural crystal structures: rutile, anatase and brookite. The structures are shown in Figure 8. Rutile is the most common and most stable of these three structures. It is also chemically inert and it can be excited by visible and ultraviolet light. Brookite and anatase are metastable forms. Anatase turns into rutile at high temperatures and it can be excited only by ultraviolet light. Brookite cannot be excited by light. Also, brookite can turn into rutile by heating. Anatase turns into rutile in air around 600 °C. Nevertheless, the transformation temperature varies between 400 and 1200 °C depending on several factors, such as the processing method, raw material and transition temperature determination method [32, 33].

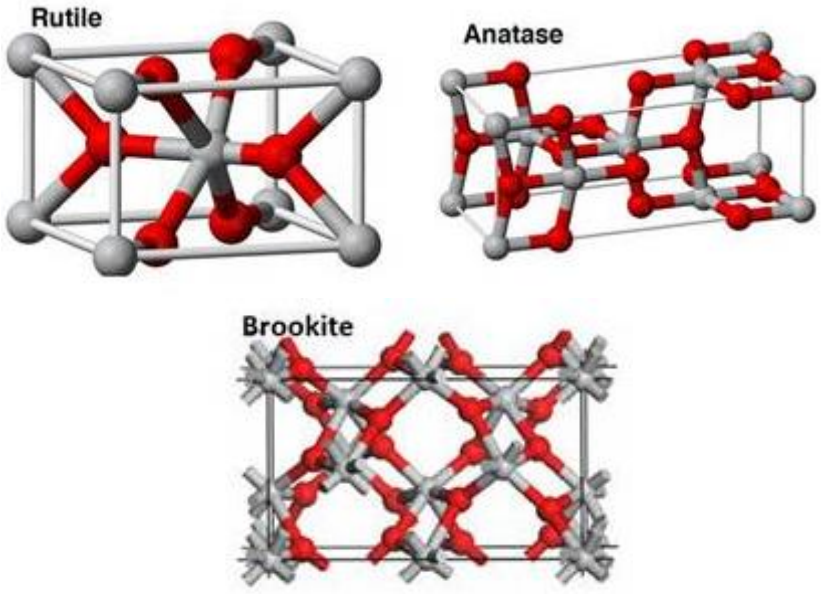

Figure 8. *Crystal structures of rutile, anatase and brookite. Titanium atoms are depicted as gray spheres, while oxygen atoms are depicted as red spheres [32].*

Titania is most often used in anatase- or rutile-forms in mesoscopic solar cells [7]. Anatase titania particles have been the most successfully used nanostructure in the mesoscopic perovskite solar cells. Nevertheless, the devices with rutile particles have higher electron diffusion coefficients and lower electron recombination. In addition to nanoparticles also other structures, such as nanorods and nanosheets, has been studied.

Other metal oxides, such as zinc oxide (ZnO) and alumina (Al_2O_3), are also used in mesoporous perovskite solar cells [7]. In this work only *n*-type anatase titania is employed as the metal oxide mesoporous layer material.

2.5.3 Hole transport layer

Holes travel along the hole transport materials to the metal cathode. HTMs are in theory not mandatory in perovskite solar cells. However, their use results in higher efficiencies in perovskite solar cells, which makes them essential in an efficient cell. HTMs prevent the back electron transfer and lead to higher fill factors and open circuit voltages. Both organic and inorganic hole conductors can be used as HTMs [34].

A capping layer of HTM is needed for high-performance perovskite solar cells to hinder the contact between the perovskite and cathode. Ideally, HTM should have a high hole-mobility, and good thermal- and UV- stabilities. It should also match with the HOMO level of the perovskite [16].

At present, 2,2',7,7'-tetrakis(N,N-di-p-methoxyphenylamine)-9,9'-spirobifluorene (spiro-OMeTAD) remains the best performing and most widely used HTM candidate for perovskite solar cells [7]. Its molecular structure is presented in Figure 9. However, spiro-OMeTAD is prohibitively expensive because of its onerous multistep synthesis that requires low temperature (-78 °C), and because of the sensitive (n-butyllithium or Grignard reagents) and aggressive (Br_2) reagents involved in the synthetic scheme. This inhibits its up-scale application in photovoltaic industry. From the commercialization viewpoint, the development of efficient yet cost-effective HTMs remains the key challenge for further advancement of the hybrid perovskite solar cells technology [35].

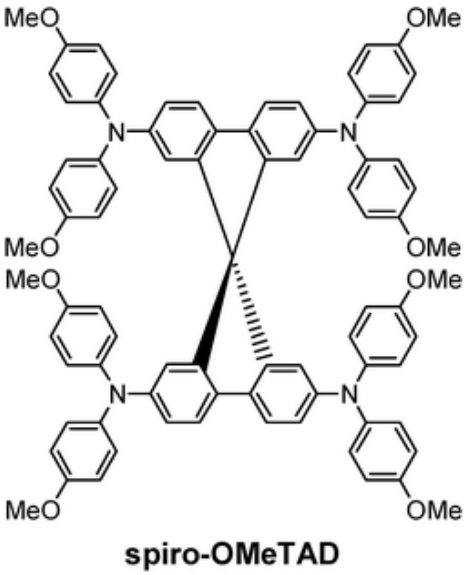

Figure 9. *The structural formula of spiro-OMeTAD.*

If spiro-OMeTAD would be used as HTM in its pristine form, the resulting solar cells would have a high series resistance, having spiro-OMeTAD poor charge transport properties. In fact, spiro-OMeTAD is typically combined with *p*-dopants, to enhance the charge transport properties [15]. *p*-doping is a method to enhance the conductivity of organic semiconductors by creating additional charge-carriers, which results in higher charge-carrier density [36].

HTM conductivity can be improved by chemical oxidants, such as tris(2-(1*H*-pyrazol-1-yl)pyridine)cobalt(III) in FK 102 Co(III) PF6 salt. Co(III) complexes are efficient *p*-dopants of spiro-OMeTAD, and their addition leads to lower series-resistance in the solar cell [26, 36, 37].

Bis(trifluoro-methane)sulfonimide lithium salt (LiTFSI) and tert-butyl pyridine (tBP) are commonly used additives. Li cations increase the conductivity of spiro-OMeTAD via a catalyzed oxidative process. LiTFSI increases significantly the conductivity and the hole mobility of spiro-OMeTAD. The open circuit voltage of solar cells is increased by addition of tBP. Li cations and tBP affect several processes in the solar cells such as the electron transport and the recombination rates. Their overall effect on HTM is complex and its detailed description goes beyond the scope of this work [26, 38].

The molecular structures of the commonly used dopants, LiTFSI, tBP and FK 102 Co(III) salt, are presented in Figure 10. These 3 dopants are employed in the solar cells fabricated in this work.

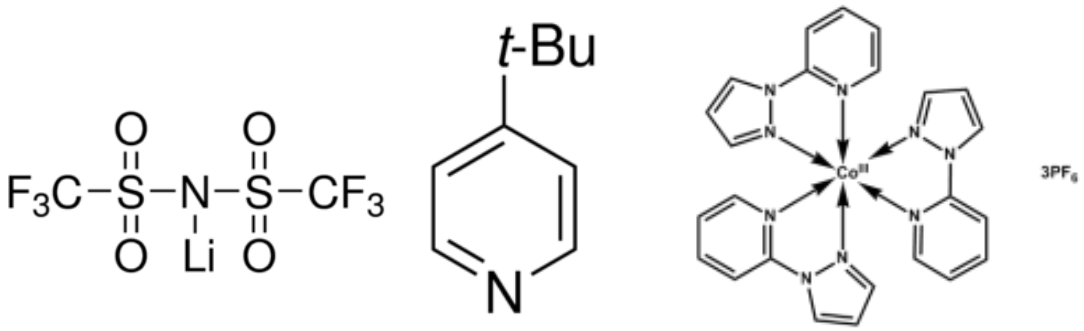

Figure 10. *The structural formulas of LiTFSI, tBP, and FK 102.*

As already mentioned, it is not mandatory to use HTMs in perovskite solar cells. Since perovskite acts both as a light harvester and hole conductor, a *p-n* junction can be formed between *n*-type metal oxides and perovskite in mesoscopic perovskite solar cells. The absence of HTM might enhance the stability, lower the production costs and facilitate the fabrication [7]. If the HTM is left out, the perovskite layer should be thick and have smooth surface to avoid shunt contacts and ensure good back contact for high-performance devices [39].

2.5.4 Counter electrode

The counter electrode collects the electrons from the external circuit and the holes transported by the HTM. It should have high conductivity for charge transport, good electrocatalytic activity, and high stability. The most common counter electrode materials are noble metals, such as platinum, silver and gold. Particularly, gold and silver are effective hole collectors to be used with the commonly adopted HTM materials. The drawback for the employment of noble metals is their high cost [40].

2.6 Characterization and evaluation of solar cells

It is important to evaluate the solar cell performances with reliable measurements, in order to compare different materials and technologies. There are several parameters, which characterize the performance of solar cells, such as the short circuit current density, the open circuit voltage, the fill factor, and the energy conversion efficiency [41].

The wavelength range emitted by the Sun goes from the ultraviolet and visible to the infrared. Ozone of the atmosphere filters out part of the ultraviolet light. Water and carbon dioxide filters out mainly the infrared light and cause some dropped peaks to the solar spectrum. The Sun has the shortest path length through the atmosphere when it is directly overhead. In that case, the maximum radiation can strike the Earth if the sky is clear. The path length is called the *air mass* (AM). Its approximated value is

$$\mathrm{AM} = \frac{1}{cos\varphi}, \tag{2.1}$$

where φ is the angle of elevation of the Sun. The standard solar spectrum is AM 1.5 G (global) for the solar cell efficiency measurements. The spectrum is normalized in a way that the integrated irradiance, radiant energy flux per unit area, is 1000 W m^{-2}. Sunlight scatters in the atmosphere, thus causing light diffusion. The fraction of the diffuse light is on average 15 %. Rough surfaces can collect the diffuse light better than the flat ones [2]. The AM1.5G solar irradiation spectrum is presented in Figure 11.

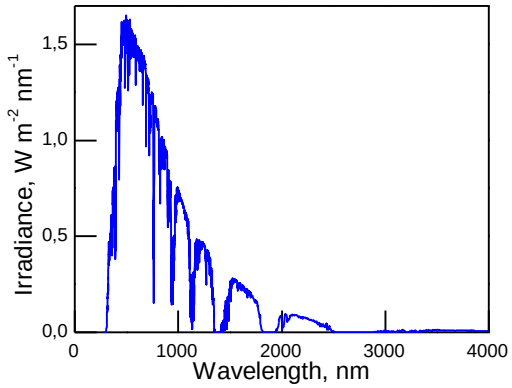

Figure 11. *Solar irradiation spectrum [42].*

Traditionally, the performance of solar cells is evaluated by measuring their current-voltage (*I-V)* characteristics. In the measurement photocurrent values of photocurrent are recorded as the bias voltage is changed stepwise. The short circuit current, I_{sc}, and the open circuit voltage, V_{oc}, can be directly determined from the recorded *I-V* curve. The short circuit current density, J_{SC} is obtained by dividing the short circuit current by the irradiated area [41]. The short circuit current density gives the maximum current density, which can be obtained from the solar cell at short circuit conditions [23]. Other important parameters, such as the fill factor, *FF*, and the energy conversion efficiency, η, can be determined using the *I-V* measurement data [41]. A *J-V* curve is depicted in Figure 12, where the open circuit voltage, the short circuit current density, and the maximum power point are also indicated.

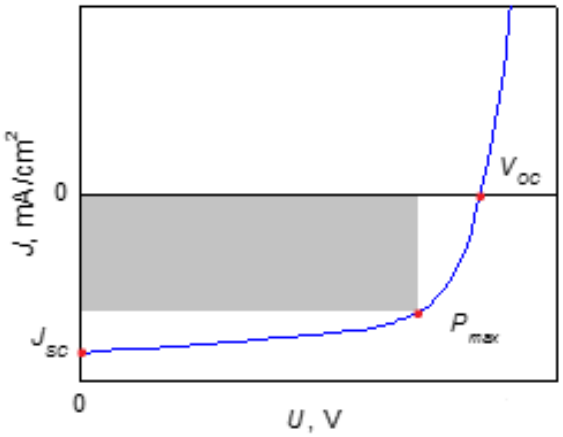

Figure 12. *J-V curve.*

In Figure 12, P_{max} is maximum power, i.e. the product of photocurrent and photovoltage at that voltage where the power output is at its maximum. The fill factor indicates the 'squareness' of the *J-V* curve [23]. Its value can be determined from the equation

$$FF = \frac{P_{max}}{I_{SC}V_{OC}}. \tag{2.2}$$

The value of the fill factor lies between 0 and 1 [2]. The ideal value is 1, but in practice this cannot be achieved due to physical constraints on diode quality in the solar cell. The main reason for the deviation from the ideal behavior is the recombination occurring at the junction, which can be described in terms of series and shunt resistances. The increase in the series resistance indicates poor conductivity through the active layers and reduced charge carrier injection to the electrodes. The reduced shunt resistance is due to either imperfections within the photoactive layers or current leaks at the interface between layers in the solar cell [23].

The energy conversion efficiency is

$$\eta = \frac{I_{SC}V_{OC}FF}{P_{in}A_{cell}} = \frac{J_{SC}V_{OC}FF}{P_{in}}, \tag{2.3}$$

where P_{in} is the irradiance of the incident light to the surface of a cell, A_{cell} is the area, which is irradiated by incident light [41]. The record efficiency for perovskite solar cells is 20.1 ± 0.4 %. The champion cell has open circuit voltage of 1.059 V, the short circuit current density of 24.65 mA/cm^2, and the fill factor of 77 % [5].

Solar cells can be also characterized with incident photon-to-current conversion efficiency, IPCE, i.e. external quantum efficiency. IPCE describes the photocurrent density produced in the external circuit under monochromatic illumination divided by the photon flux, $e\Phi$, which encounters the cell. IPCE is determined as

$$\text{IPCE} = \frac{J_{SC}(\lambda)}{e\Phi(\lambda)} = 1240\frac{J_{SC}[A\ cm^{-2}]}{\lambda[nm]P_{in}(\lambda)[W\ cm^{-2}]}, \tag{2.4}$$

where λ is the wavelength [2].

2.6.1 Measuring perovskite solar cell performance

There are various factors to be taken into consideration in order to measure the performance of perovskite solar cells accurately. The main issue is the hysteresis in *I-V* curves, which is affected by the measurement setup and by the solar cell construction. The hysteresis is different for every cell. The origin of the hysteresis is not yet understood. Erroneous interpretation and representation of the performances can be avoided by following certain guidelines [6, 43].

In general, the *I-V* curves are obtained by sweeping the potential difference between the working and counter electrode and monitoring the current response simultaneously. The sweep rate should be carefully selected for each device. If the sweep rate is faster than the response time of the device, the recorded curve does not show steady-state performance. The direction of the sweep causes hysteresis in the *I-V* curves. Figure 13 shows the effect of the sweep rate. The steady-state output gives the actual values. Figure 13 presents also the effect of scan direction. The real output of the device lies between the forward and reverse scan curves [43].

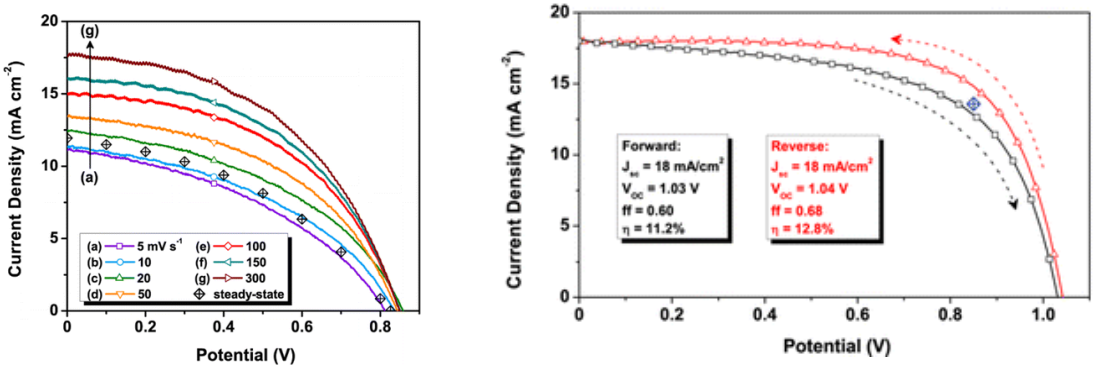

Figure 13. *An example of the effect of the sweep rate (left) and scan direction (right) to the J-V curve [43].*

The measured current density values can be verified by measuring and integrating the IPCE spectra over the AM1.5G solar spectrum. The integrated current density is

$$J_{SC,INT} = \frac{F \times \int(E_{e\lambda} \times IPCE)\mathrm{d}\lambda}{N_A}, \tag{2.5}$$

where N_A is the Avogadro constant, F the Faraday constant, and $E_{e\lambda}$ the solar spectral irradiance. The integrated and measured current density values should be approximately equivalent if the measurements have been executed carefully [43].

The solar cells should be masked right before the measurements. This avoids the under- and overestimations of the cell performance [43]. A mask should have a single aperture through which the light enters the cell. This prevents the light entering the cell from elsewhere [44].

To conclude, the following recently published guidelines should be followed when an accurate evaluation of the devices performance is desired. The measured cell needs to be masked, the measurement position should be always exactly same, and the illumination source must be calibrated. The steady-state values for J_{SC} and V_{oc} have to be determined, and the stability monitored. *J-V* should be measured at various scan rates in both forward and reverse directions. The determined current density is finally checked by calculating the corresponding value from the IPCE data [43, 44].

3. MATERIALS AND METHODS

This work studies titania anode in perovskite solar cells. This Section focuses on the fabrication and the research methods of samples analysed in the Thesis work. The adopted research methods are scanning electron microscopy, steady-state absorption and reflectance spectroscopies, and *I-V* measurements. The experimental part of this work was carried out during summer and autumn 2015 at the 'supramolecular photochemistry' laboratory of Tampere University of Technology. The self-made titania anodes are applied for the first time in perovskite solar cells at TUT in this work. The fabrication and measurement methods follow the most up-to-date and precise protocols and guidelines published in the literature.

3.1 Sample preparation

The construction of the samples is performed in a clean room with ISO6 classification. All the samples are built on conducting fluorine tin oxide (FTO)-covered glass slides. The size of the FTO substrates (TEC7, Solems) is 2 x 2 cm, their square resistance is 6-8 Ω, and the thickness of the FTO layer is 600 nm. The substrates are cleaned and etched prior use.

Etching is performed in order to remove part of FTO and prevent direct contact between the working and counter electrodes. The part of the FTO substrate is limited with Kapton tape. The tape is installed so that approximately 5 mm wide stripe is left uncovered on the bottom of the substrate. FTO is etched with Zn powder and HCl from the uncovered part. The Zn powder is spread on the surface of the area to be etched. Then a few drops of 4 M HCl solution are released on the surface of zinc. They are let to react for a couple of minutes followed by rubbing with a brush. After removing the tapes the substrates are wiped with ethanol (EtOH).

After etching, the substrates are cleaned mechanically and chemically. The substrates are brushed mechanically with 2 % Hellmanex III cleaning solution which is followed by sonication in 2 % Hellmanex solution for 15 min. Then the substrates are rinsed with MilliQ water and ethanol. The cleaning is continued with sonication in 2-propanol (IPA) for 15 min and rinsing with acetone. Finally the substrates are dried under nitrogen flow.

UV-ozone treatment is performed immediately before the deposition of the first layer on top of FTO substrates. The treatment is done in order to remove organic residuals from

the surface. The substrates are cleaned with UV-ozone cleaner (ProCleaner, BioForce Nanosciences) for 15 min.

3.1.1 Materials and solution preparations

The structure of the prepared solar cells is shown in Figure 14. Titania, perovskite and hole transport material layers are solution-processed layers in the solar cells. Gold is evaporated thermally from solid particles.

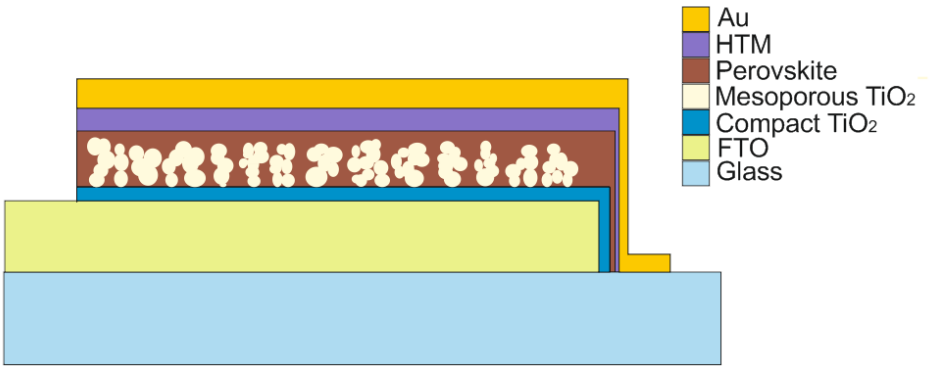

Figure 14. *Mesoscopic perovskite solar cell structure.*

Precursor solutions for TiO_2 compact layer are prepared from titanium tetrachloride or titanium isopropoxide. 2 M solution of $TiCl_4$ is prepared by dissolving liquid $TiCl_4$ in MilliQ water in an ice bath under vigorous stirring. 175 µl of titanium isopropoxide is first dissolved in 1.25 ml of anhydrous ethanol or 2-propanol. This solution is added dropwise under stirring to a solution which contains 1.25 ml of anhydrous ethanol or 2-propanol and 17.5 µl of 2 M HCl.

The solution for TiO_2 mesoporous layer is prepared from TiO_2 18 NR-T paste (Dyesol) having the titania particle size of 20 nm. The paste is dissolved in ethanol using weight ratios 2:7 or 2:9. The paste is dissolved using a Vortex mixer and stirred overnight in order to ensure a homogenous particle distribution in the solution. The weight ratio 2:7 is used for 300 and 400 nm thick titania layers, while 2:9 for the 190 nm thick mesoporous titania film.

Perovskite is depostited by using the lead iodide (PbI_2) and methyl ammonium iodide (MAI) solutions. 1 M PbI_2 solution is prepared by dissolving PbI_2 in anhydrous dimethyl formamide at 120 °C for 1 h under continuous stirring. Then the solution is kept at 70 °C under stirring to prevent the crystallization of PbI_2. 10 mg/ml MAI solution is prepared by dissolving MAI in anhydrous 2-propanol and stirred for 15 min at room temperature. The MAI solution is prepared just before its use since it is highly sensitive to the moisture.

The hole transport layer is prepared from 2,2',7,7'-tetrakis-(N,N-di-4-methoxy-phenylamino)-9,9'-spirobifluorene (Spiro-OMeTAD) and dopants: bis(trifluoro-methane)sulfonimide lithium salt (LiTFSI), tert-butyl pyridine (tBP) and FK 102 Co(III) PF6 salt. The recipe is taken from Burschka *et al.*(Ref. [37]). The HTM solution preparation starts by making the LiTFSI and FK 102 stock solutions. The LiTFSI stock contains 520 mg/ml of LiTFSI in acetonitrile. The FK 102 stock is prepared by dissolving 300 mg FK 102 salt in acetonitrile. Spiro-OMeTAD is dissolved in anhydrous chlorobenzene with concentration 72.3 mg/ml. The dopants are added as follows: 17.5 µl of LiTFSI stock, 28.8 µl of tBP and 29 µl of FK 102 stock to 1 ml of spiro-OMeTAD solution in this order. The solution is stirred for 10 min and is used as freshly made for spin-coating.

3.1.2 Spin-coating

Spin-coating is an easy method used to deposit a thin solid layer of desired material from solutions on the substrate. The film precursor solution is applied on the substrate. The film is formed as the centrifugal force spreads the solution and spins the solvent off the substrate, when the substrate is spun.

The layers which are prepared by spin-coating in the present work are compact and mesoporous TiO_2, PbI_2 and hole transport layer (HTL). The areas of the spin-coated films are limited to approximately 1 cm wide with Kapton tape. Before spin-coating the FTO substrates are blown with nitrogen to remove possible dust particles from the surface. Spin-coating is performed with Laurell WS-400B-6NPP/LITE spin-coater. All the spin-coating parameters are listed in Table 1.

Table 1. *Spin-coating parameters for each spin-coated layer.*

Layer	Rotation speed (rpm)	Angular acceleration (rpm/s)	Duration (s)	Solution volume (µl)
compact TiO_2	3000	3000	30	70
190 nm mesoporous TiO_2	5000	5000	30	65
300 nm mesoporous TiO_2	5000	2000	30	65
400 nm mesoporous TiO_2	2500	2000	30	65
PbI_2	6100	6000	30	60
HTM	4000	4000	30	50

Prior testing different compact titania layer precursor solutions in solar cells, their film formation was tested. The titanium tetrachloride in water and titanium isopropoxide in ethanol and in isopropanol were spin-coated on clean FTO substrates. The titanium isopropoxide solutions produced a smooth transparent film, with no visible flaws. The $TiCl_4$ solution generated an uneven film. Even after repeating the $TiCl_4$ solution preparation, the formation of a smooth film did not succeed. This is likely due to the degradation of the $TiCl_4$ chemical because of the heat and moisture in air. Based on the film formation tests it was decided that the $TiCl_4$ solution will not be used in further experiments.

The solar cell construction starts with spin-coating compact TiO_2 layer precursor solution on FTO. The film is dried on hot plate at 120 °C around 10 min and let to cool down to the room temperature. For some samples the spin-coating of the compact layer precursor is repeated before spin-coating the mesoporous layer. After cooling down the mesoporous TiO_2 layer is spin-coated and dried on hot plate at 125 °C for 5–10 min. The titania is then sintered in the furnace. The sintering program starts with a heating ramp of 15 °C/min, then the temperature is held at 500 °C for 30 min and then the plates are let to cool slowly down to 150 °C.

Perovskite is formed via sequential deposition on top of titania, starting from the spin-coating of PbI_2. The perovskite fabrication is described more closely in Section 3.1.3. HTM solution is spin-coated on top of perovskite. The appearance of the layers in solar cells is shown in Figure 15.

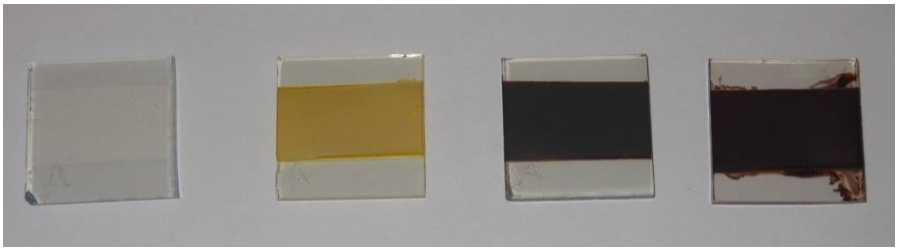

Figure 15. *The appearance of the films layer-by-layer. From letft to the right: TiO_2, PbI_2, perovskite, and HTM layers.*

After spin-coating of HTM the plates are wiped clean from the back and side with chloroform and a cotton stick. The HTM is oxidized in air for around 2.5 h prior gold electrode deposition in order to enhance the doping effects of spiro-OMeTAD with additives.

3.1.3 Sequential deposition of perovskite

Perovskite can be deposited either using one-step or two-step method. In this work methyl ammonium lead iodide perovskite, $CH_3NH_3PbI_3$ is formed using sequential deposition method in which perovskite is solution-processed in two steps. First PbI_2 is

spin-coated as described in the previous paragraph. The PbI_2 film is dried at 70 °C on hot plate for 15 min. Then the substrates are immersed vertically in the MAI solution for 20 s. Perovskite is formed in the solution as a result of the reaction between PbI_2 and MAI:

$$PbI_2 + CH_3NH_3I \rightarrow CH_3NH_3PbI_3. \quad (1)$$

After the immersion the films are rinsed with 2-propanol, to remove the unreacted MAI from the surface of perovskite. The film is dried from 2-propanol with the spin-coater, which drives the solvent off the substrate. The formed perovskite film is annealed in vacuum at 80 °C for 30 min prior the HTM deposition. Perovskite is formed in air with relative humidity of 43–45 %. The ambient temperature during the fabrication is 21 °C.

3.1.4 Thermal evaporation

Thermal evaporation is a method which produces thin and smooth films. Thermal evaporation has a good controllability of the film thickness. The material, which is used to form a film, evaporates and condensates on the surface of the substrate. In this work the thermal evaporation is used for the gold electrode fabrication, which is the final step of the solar cell construction. The substrates are masked to determine the area and shape of the electrodes. Figure 16 presents the outlook of the electrodes and the ready-made solar cells.

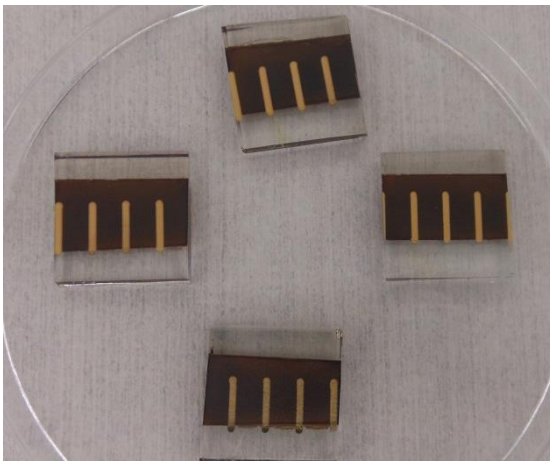

Figure 16. *Perovskite solar cells with gold electrodes.*

The masked substrates are placed into the vacuum chamber of Edwards Auto306 evaporator. Gold particles are placed onto molybdenum boat inside the vacuum chamber (pressure ≈ 10^{-6} mbar). Current is directed through molybdenum boats which generates heat and evaporates gold. The evaporation rate of gold is at first < 0.1 nm/s and towards the end the rate is lifted gradually to 0.08 nm/s. The evaporation takes approximately 60 min. The thickness of evaporated gold is 70-80 nm. The solar cells are stored in vacuum overnight after evaporation prior *I-V* measurements.

3.2 Research methods

The prepared films are characterized with scanning electron microscopy and absorption and reflectance measurements. The performance of the solar cell is characterized with *I-V* measurements.

3.2.1 Scanning electron microscopy

Scanning electron microscopy (SEM) is used to determine the thickness of the films in solar cells and to investigate the surface morphology of the samples. SEM has high resolution (~1 nm) and it is used to image and characterize small–scale details. The scanning electron microscope focuses an electron beam to the surface of the sample. The electrons interact with the surface resulting for example secondary electrons and back-scattered electrons. The electrons are detected to produce images. SEM images are taken both from the surface and the cross-section of the samples. To reveal the cross-section, the samples are cut in half before imaging. Copper tape is applied to all SEM samples before imaging to enhance the conductivity and avoid charging of the samples. In this work, the used aperture size is either 10 or 20 nm and the acceleration voltage is 2-6 V. The distance from the surface to the electron gun varies from 1.8 mm to 4.9 mm.

3.2.2 Steady-state absorbance and reflectance measurements

Absorbance and reflectance spectra of the samples are recorded after each deposited layer. Reflectance is recorded because the opacity of the samples results distortions in the absorption spectrum, since the samples have a reasonable reflectance level. Absorption spectra are recorded with UV 1800 (Shimadzu) spectrophotometer. UV 3600 (Shimadzu) spectrophotometer with integrating sphere attachment is used for reflectance measurements. Figure 17 presents the measurement setup of the integrating sphere.

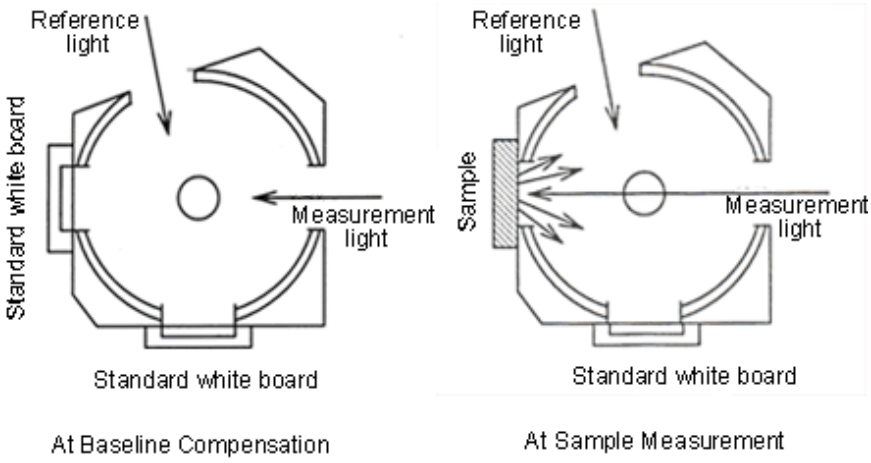

Figure 17. *A scheme of measuring reflectance with an integrating sphere [45].*

The baseline in the absorption measurements is recorded with a mask. The mask is used for each absorption measurement in order to have the same absorbing area. In this way the absorbance level of the samples can be compared to one another. The absorption spectra are recorded in the wavelength range from 300 nm to 850 nm. The reflectance spectra are recorded without masks. The area of the reflectance samples varies, hence the valuable information achieved is the shape of the spectra. The reflectance spectra are recorded in the wavelength range from 350 nm to 850 nm.

3.2.3 *I-V* measurements

I-V measurements are performed under 1 sun illumination which corresponds to solar mass AM 1.5 G. The used light source is Xe lamp (66921, Newport). A 315-710 nm bandpass filter (FGS900S, Thorlabs) is used to select the correct wavelength area. The light intensity is calibrated to AM 1.5 G with a silicon reference cell (Oriel instruments). To record the *I-V* data, Agilent E5272A source-monitor unit is used. The *I-V* measurements are carried out in ambient air. An illustration of the measurement setup is shown in Figure 18.

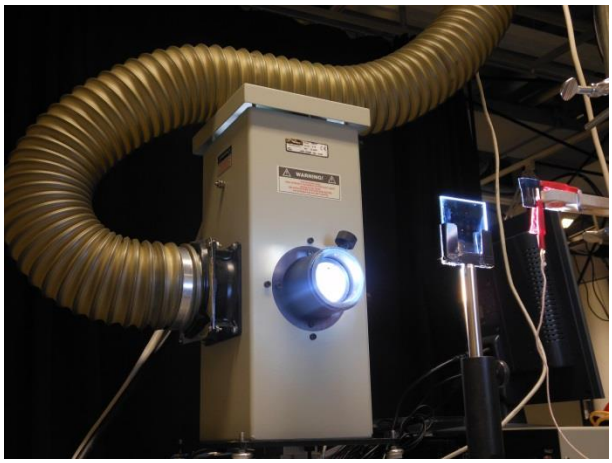

Figure 18. *I-V measurement setup.*

Prior measurement silver paint is applied to the ends of gold electrodes to make sure to have a proper contact from the gold electrodes to the cables of the source-monitor unit. Solar cells are also masked with black electrical tape to avoid possible under- and overestimations of the cell performance. With the tape the aperture area of the light is tuned to be slightly smaller than the gold electrode on top of the cell. The active area of each cell is the size of the aperture and it is determined with an optical Dino-Lite AM4113ZTL microscope.

The voltage range of the *I-V* measurements is 0–1 V. The scan rate is 10 mV/s. The low rate is chosen to avoid a remarkable overestimation of the photocurrent values, and thus of the solar cell efficiencies. The guidelines for the measurements are taken from Christians *et al.*(Ref. [43]). The scanning under illumination is first performed in the forward direction, followed by the scan in the reverse direction under illumination. To obtain the *I-V* curve in the darkness only the forward scan is performed. In the measurements the light encounters the solar cell from the glass side.

4. RESULTS AND DISCUSSION

This Section introduces the results of the measurements and their analysis. Those contain *I-V* characteristics, absorption and reflectance spectra, and SEM images. The most important conclusions are based on calculated photovoltaic parameters.

All the samples are fabricated in air with relative humidity of 43–45 %. Because of the moisture in air and other atmospheric effects, the perovskite fabrication is not totally reproducible and the degree of degradation varies. Thus, the photovoltaic parameters of the prepared solar cell series are not fully comparable to each another. The comparisons are made between samples in the same series to avoid misinterpretations.

4.1 Optimization of compact titania layer

The optimum thickness of the titania compact layer was first studied. Half of the samples had one and the other half had two coatings of the compact titania precursor solution. The solvent of the precursor was anhydrous ethanol. Every solar cell had a 300 nm thick mesoporous titania layer. Figure 19 presents *J-V* curves of two different solar cell samples having one coating of the precursor solution.

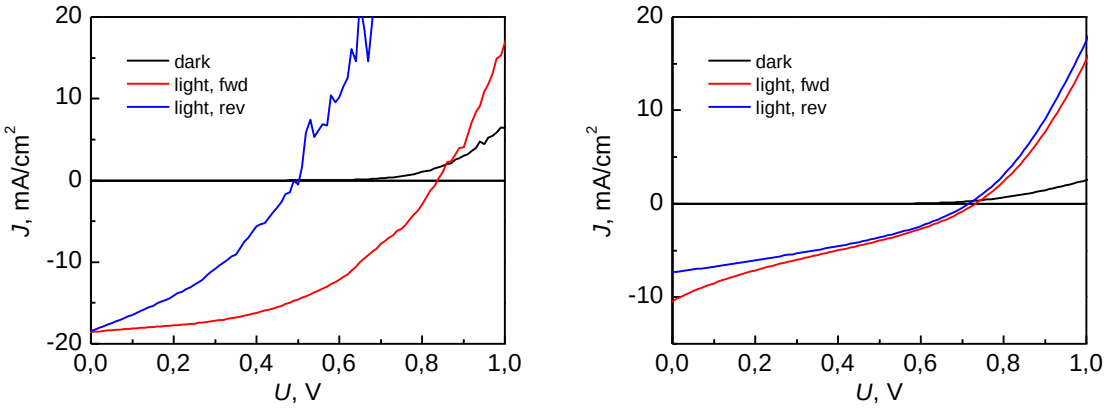

Figure 19. *J-V curves of two solar cells (sample 1 left and sample 2 right) with one coating of compact titania layer with 300 nm thick mesoporous titania layer. The solvent of the compact layer precursor was anhydrous ethanol.*

For sample 1 the forward scan under light shows reasonably good squareness of the curve, but the reverse scan rises steeply, thus demonstrating the degradation of the sample during the measurements. Sample 2 does not show as good squareness. The forward scan in light has a slight S-shape, which demonstrates that the solar cell does

not act as an ideal diode. Figure 20 exhibits the *J-V* curves of the samples with two coatings of compact titania precursor solution.

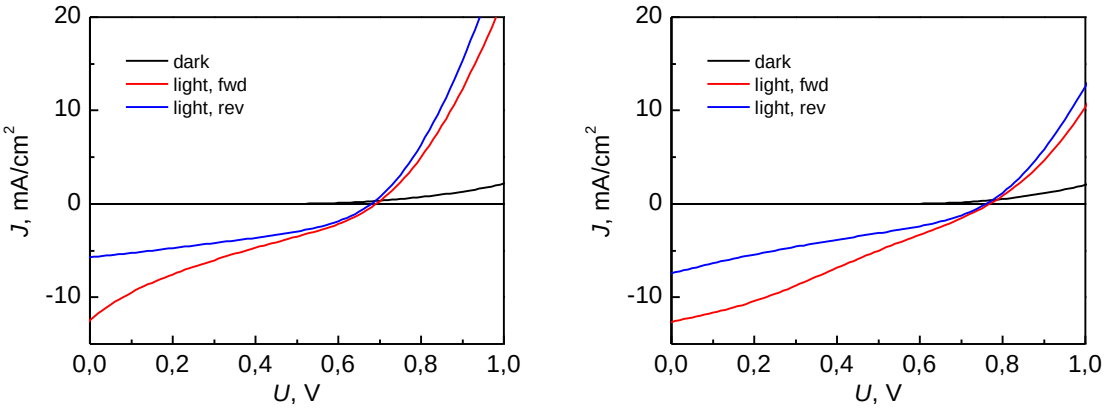

Figure 20. *J-V curves of the solar cells (sample 3 left and 4 right) with two coatings of compact titania layer and 300 nm thick mesoporous titania layer. The solvent of the compact layer precursor was anhydrous ethanol.*

Sample 3 demonstrates a more evident S-shape than the solar cells in Figure 19. In the right graph the linear trend in both *J-V* curves might indicate an increased resistance for electron injection to the FTO electrode. This could be explained by thicker titania compact layer coating through which the electrons have to pass to reach the electrode. The photovoltaic parameters for testing the thickness of the titania compact layer in solar cells series are collected in Table 2.

Table 2. *The photovoltaic parameters of the solar cells with one or two coatings of compact titania layer precursor and 300 nm thick mesoporous titania layer. The solvent of the compact layer precursor was anhydrous ethanol. The sample numbering correspond to those of Figure 19 and Figure 20.*

Sample	Number of coatings	Scan direction	η (%)	*FF* (%)	J_{sc} (mA/cm2)	V_{oc} (V)
1	1	forward	7.42	48.06	18.61	0.83
1	1	reverse	3.28	35.60	18.44	0.50
2	1	forward	5.03	42.22	14.37	0.83
2	1	reverse	4.50	43.97	12.64	0.81
3	2	forward	1.89	21.92	12.49	0.69
3	2	reverse	1.49	38.98	5.72	0.67
4	2	forward	2.95	28.66	13.56	0.76
4	2	reverse	1.69	28.11	8.00	0.75

The photovoltaic parameters show that the efficiency is moderate for the solar cells with one coating, if considering that the solar cells were fabricated in the presence of moisture in air. Their fill factor is modest compared to the record efficiency perovskite

solar cell (Ref. [5]) having the fill factor 77 %. This is also the case for the open circuit voltages and short circuit currents. The solar cells with two coatings have poor efficiencies. Also the fill factor and short circuit current are low. The open circuit voltage decreased with second coating.

Cross-sectional SEM images were recorded for the sample with one coating of compact titania layer (Sample 1), Figure 21. The SEM image shows that the thickness of compact layer is approximately 40–50 nm. The thickness has some variation since the FTO surface is rough. It has been reported that optimum thickness is about 80–100 nm prepared by the spin-coating method, while a thicker compact layer should be avoided because it increases resistance [47, 48]. However, also thinner compact layers are employed. For example Burschka *et al.* have used 30 nm thick compact titania layer prepared by spray-pyrolysis [37]. The deviations in the reported thicknesses might be due to the fact that spray-pyrolysis forms more uniform films with less pinholes than those produced by spin-coating. To conclude, the thickness of the compact layer leading to the best-performing solar cells in this work is in the same range than the thicknesses in the literature.

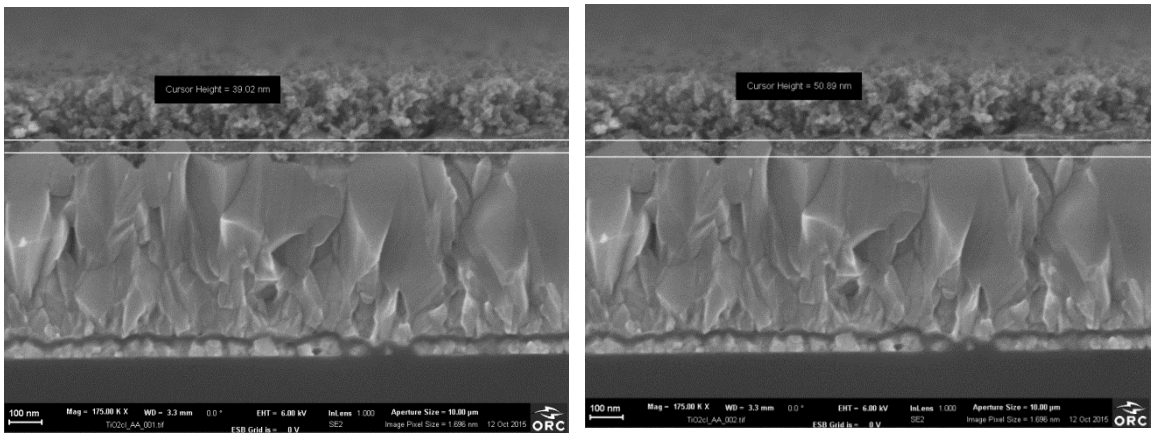

Figure 21. *SEM images of the sample with one coating of compact titania layer between FTO (bottom layer) and mesoporous titania layer(top). The solvent of the compact layer precursor was anhydrous ethanol.*

Next it was studied if the anhydrous ethanol in the compact layer precursor solution could be replaced with 2-propanol. For this series only one coating of the compact titania precursor solution was used. The mesoporous layer thickness for these cells was 300 nm. *J-V* curves of the solar cells are presented in Figure 21.

Figure 22 shows fairly that the all four solar cells have quite good shapes using either solution. The *J-V* curves of the samples 1 and 4 have some contact problems and signs of degradation, as evident from the fluctuation in the curves. Based on the *J-V* characterization it can be suggested that titanium isopropoxide in anhydrous ethanol is a better solution to produce high-performance solar cells.

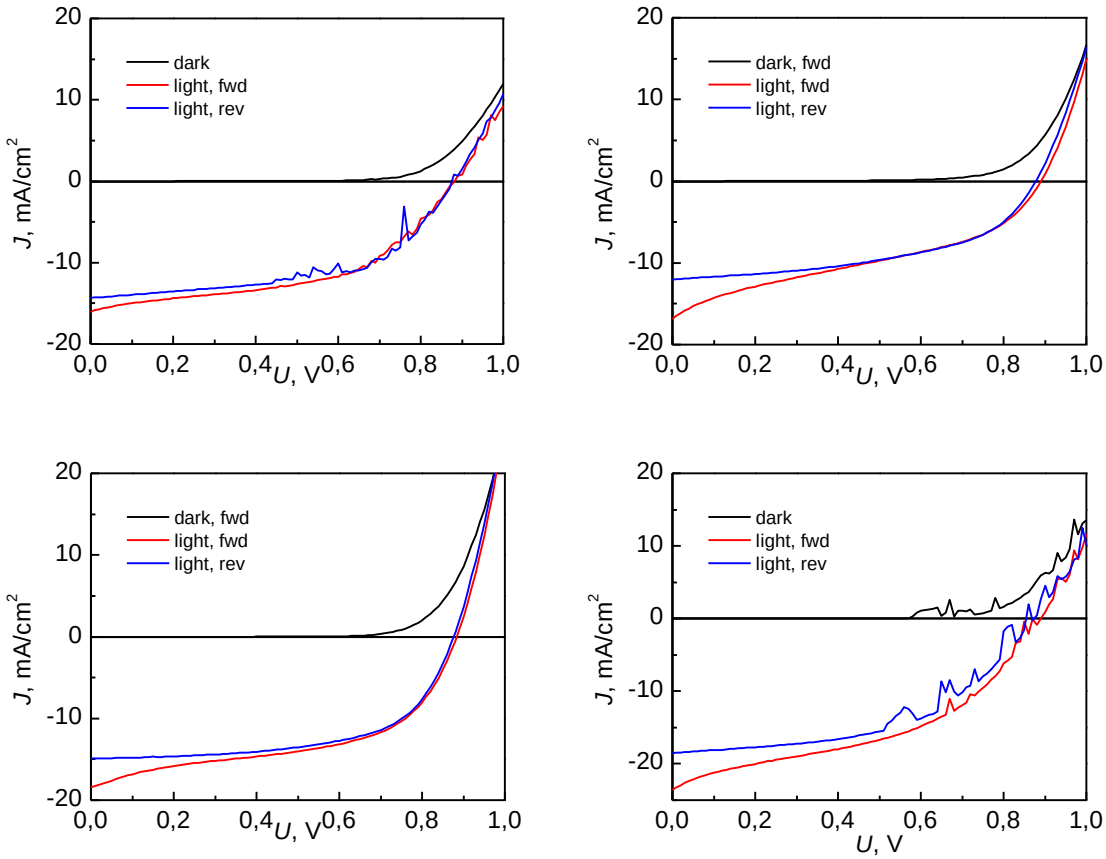

Figure 22. *J-V curves of the solar cells with 2-propanol as the solvent of compact titania layer precursor solution (sample 1 top left and sample 2 top right), and anhydrous ethanol as the solvent (sample 3 bottom left and sample 4 bottom right).*

The photovoltaic parameters of these solar cells are shown in Table 3. As predicted, the devices with titania precursor in EtOH have enhanced performance and their efficiencies are closer to one another. However, 2-propanol cells have also reasonable efficiencies and thus isopropanol can still be used if no anhydrous ethanol is available. The open circuit voltage values for all the cells are almost the same. The short circuit current is higher for the cells with the precursor in ethanol. This could be due to lower pinhole concentration in the compact layer film.

Table 3. *The photovoltaic parameters of the solar cells with anhydrous ethanol and 2-propanol as the compact layer solvent. The sample numbering correspond to those of Figure 22.*

Sample	Solvent	Scan direction	η (%)	*FF* (%)	J_{SC} (mA/cm2)	V_{OC} (V)
1	IPA	forward	7.11	50.32	16.05	0.88
1	IPA	reverse	7.14	57.29	14.33	0.87
2	IPA	forward	5.26	35.10	16.38	0.89
2	IPA	reverse	5.31	50.65	12.04	0.87
3	EtOH	forward	8.21	50.70	18.40	0.88
3	EtOH	reverse	7.98	61.70	14.87	0.87
4	EtOH	forward	8.91	42.88	23.62	0.88
4	EtOH	reverse	8.27	51.30	18.52	0.87

Compared to the record efficiency perovskite cells (Ref. [5]), in this series fill factors are not very high but they are indeed better than in the first solar cell series. Instead, the open circuit voltages are relatively high.

SEM images were recorded from the compact layer prepared from titanium isopropoxide in isopropanol, Figure 23, in order to evaluate the presence of pinholes in the film. Based on the SEM image, the compact layer was uniform. If there were some pinholes the resolution of SEM was not high enough to see them.

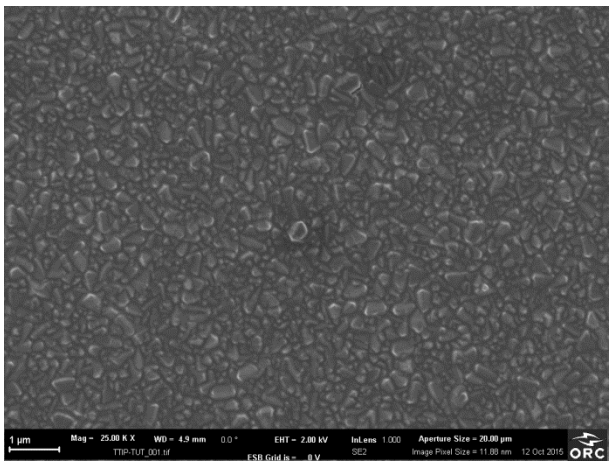

Figure 23. *SEM image of compact titania prepared from titanium isopropoxide in isopropanol from the top.*

To estimate the thickness of the film produced with the precursor in isopropanol, cross-sectional SEM images were recorded and shown in Figure 24. Also this solution produced films with the average thickness between 40–50 nm.

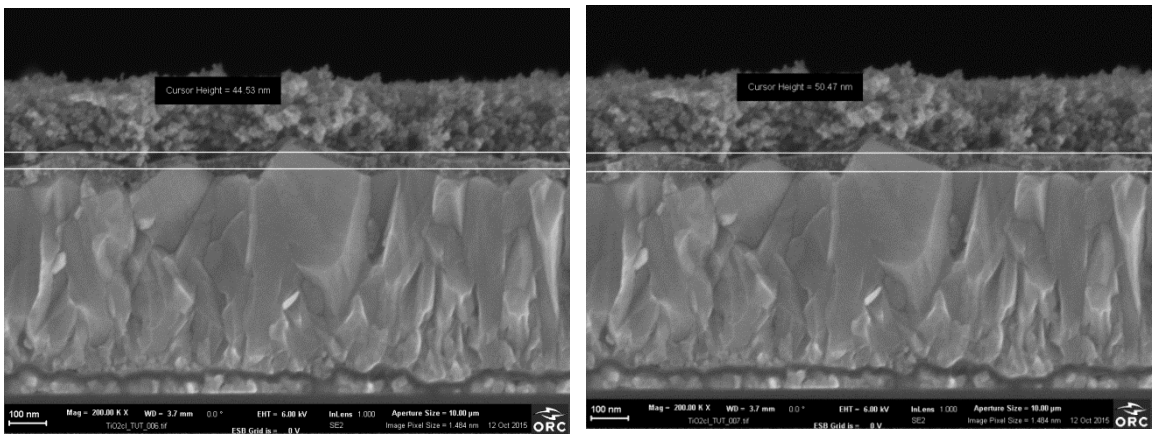

Figure 24. *SEM images of the sample with one coating of compact titania layer precursor in isopropanol between FTO (bottom layer) and mesoporous titania layer.*

According to the test results, the best solution to produce the compact layer by spin-coating was titanium isopropoxide in anhydrous ethanol. One coating of the solution produced the best-performing solar cells. This recipe and one spin-coating round is also employed by Pathak *et al.*(Ref.[48]). It was decided to use this solution for the remaining experiments of this Thesis.

4.2 Optimization of mesoporous titania layer

Scanning electron microscopy and absorption spectroscopy, together with the *I-V* measurements of solar cells, are employed to optimize the thickness of the mesoporous titania layer. First the thickness of the mesoporous titania, prepared with different spin-coating parameters, was optimized. Figure 25 shows three cross-sectional SEM images of samples with different mesoporous titania thicknesses and one top image to illustrate the porosity of the layer, and the nanoparticle distribution. The thicknesses of the mesoporous titania layers are approximately 190, 300 and 400 nm. The top image shows that the nanoparticle distribution is uniform.

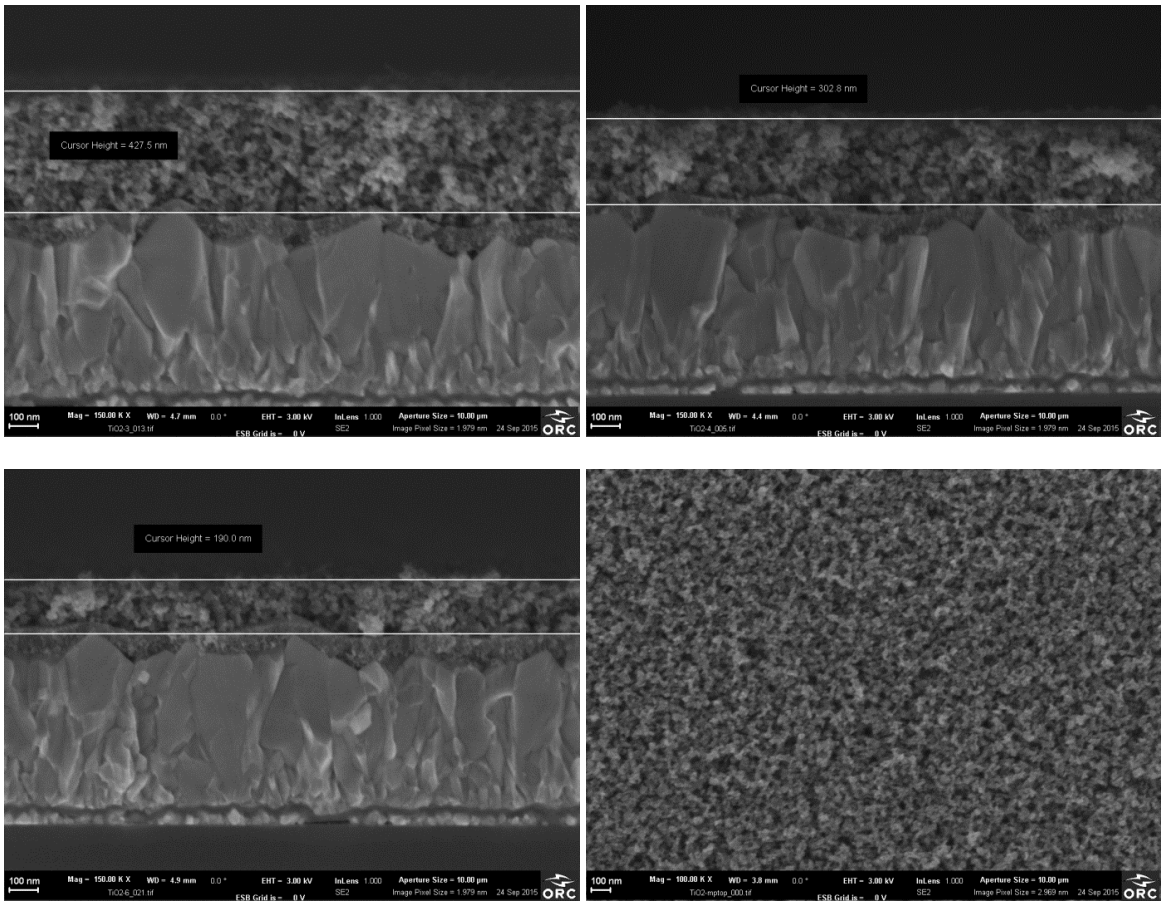

Figure 25. *Cross-sectional SEM images of samples with 190, 300 and 400 nm thick mesoporous titania layers on top of FTO substrate coated with compact titania layer and top image (bottom right) of the mesoporous layer.*

Figure 26 depicts the absorption spectra of the samples with different thicknesses of mesoporous titania. Because the titania layers are very thin, the absorbance level of the samples can be interpreted to be the same within the measurement accuracy. The absorbance level of all the samples is close to 0.1 in the visible range. This means that the transmittance is around 0.79 according to the Equation (3). Hence, 79 % of the visible light reaches the perovskite layer in the solar cells.

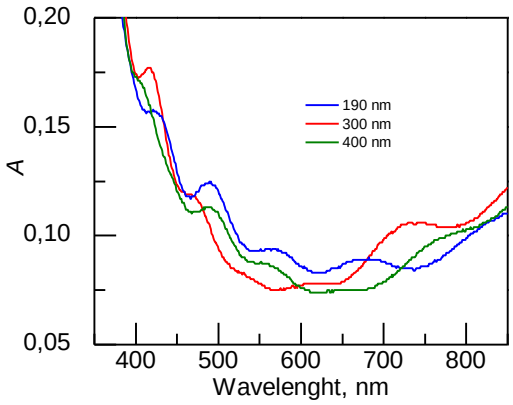

Figure 26. *Absorption spectra of the mesoporous titania layer with different thicknesses.*

The first series of solar cells for the mesoporous layer optimization consists of samples with 300 and 400 nm thick mesoporous layers. Figure 27 presents the *J-V* curves of these cells. The *I-V* data is measured right after taken the samples out of the vacuum.

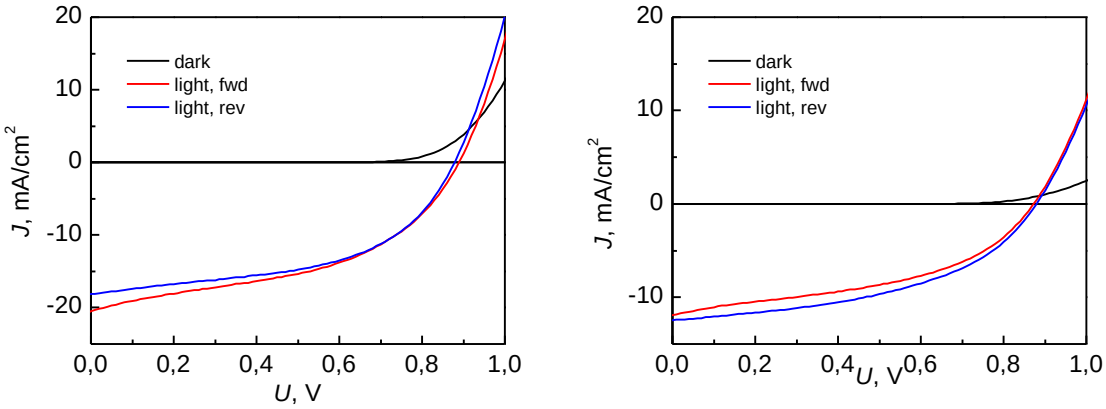

Figure 27. *J-V curves of the solar cells with 300 nm (left) and 400 nm (right) thick mesoporous layer immediately after taken out of vacuum.*

The photovoltaic parameters of the solar cells for testing the mesoporous thicknesses are shown in Table 4. The efficiency with 300 nm thick mesoporous layer is clearly higher than with 400 nm thick mesoporous layer. This is mainly due to the high fill factor and the short circuit current values. The difference in the open circuit voltages between these two thicknesses is negligible.

Table 4. *The photovoltaic parameters of the solar cells with 300 nm and 400 nm thick mesoporous titania layers immediately after taken out of vacuum.*

Sample	Thickness of mesoporous TiO_2 (nm)	Scan direction	η (%)	*FF* (%)	J_{SC} (mA/cm2)	V_{OC} (V)
1	300	forward	8.34	46.17	20.51	0.88
1	300	reverse	8.16	51.68	18.14	0.87
2	400	forward	6.08	40.33	16.75	0.90
2	400	reverse	5.60	40.82	15.58	0.88

The degradation of the perovskite solar cells with different thicknesses of the mesoporous titania layers was tested by recording the *I-V* curves of the same samples after one week from the fabrication. The devices had been stored in darkness in ambient air with relative humidity around 44 %. The *J-V* curves are shown in Figure 28, and the photovoltaic parameters in Table 5.

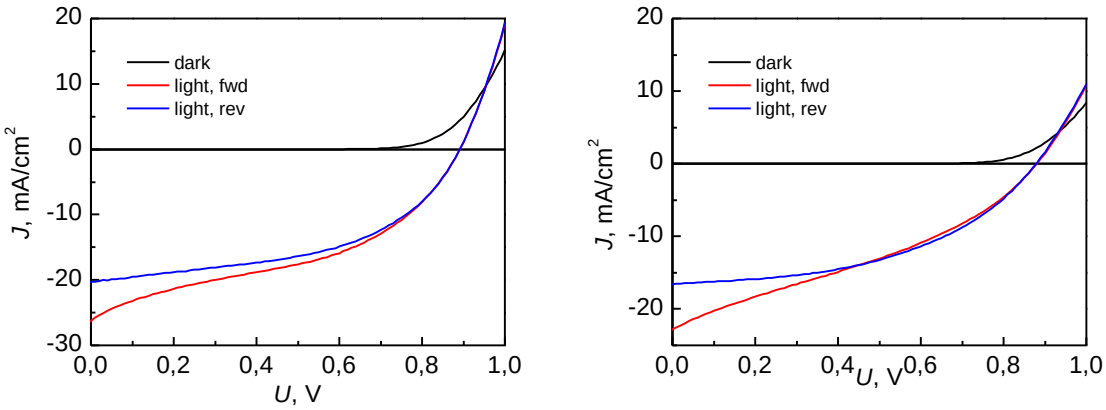

Figure 28. *J-V curves of the solar cells with 300 nm (left) and 400 nm (right) thick mesoporous layer immediately after one week of storage* in darkness.

The efficiencies are higher after one week storing. This kind of phenomenon for perovskite solar cells is mentioned rarely in the literature. The increase might be due to better contact at the interface of the HTM and the metal electrode, as it is suggested for dye-sensitized solar cells in Ref. [36].

The short circuit currents are remarkably high after one week storing. This might be due the improper masking during the *I-V* measurements. The currents are quite high also immediately after taken out of the vacuum but did not raise suspicion of overestimation. After one week one of the short circuit currents is even higher than that of the best perovskite cell of the series. The masking is not changed in between the measurements. Despite the possible overestimation, conclusions can be drawn based on the tendency of the photovoltaic parameters. The efficiency difference is also significant enough that, despite some inaccuracy, it is safe to say that 300 nm thick mesoporous titania layer is

better than 400 nm thick one for high-performance mesoscopic perovskite solar cells. The increase in efficiency in time is an interesting phenomenon which should be studied more.

Table 5. *The photovoltaic parameters of the solar cells with 300 nm and 400 nm thick mesoporous titania layers after storing for one week.*

Sample	Thickness of mesoporous TiO_2 (nm)	Scan direction	η (%)	*FF* (%)	J_{SC} (mA/cm2)	V_{OC} (V)
1	300	forward	9.55	40.91	26.22	0.89
1	300	reverse	8.99	49.73	20.32	0.89
2	400	forward	6.84	47.44	16.57	0.87
2	400	reverse	6.63	33.41	22.80	0.87

The effect of thicknesses was further tested for a solar cells series with 190, 300 and 400 nm thick mesoporous titania layers. The *J-V* curves of the solar cells with 190, 300 and 400 nm thick mesoporous layers are shown in Figure 29.

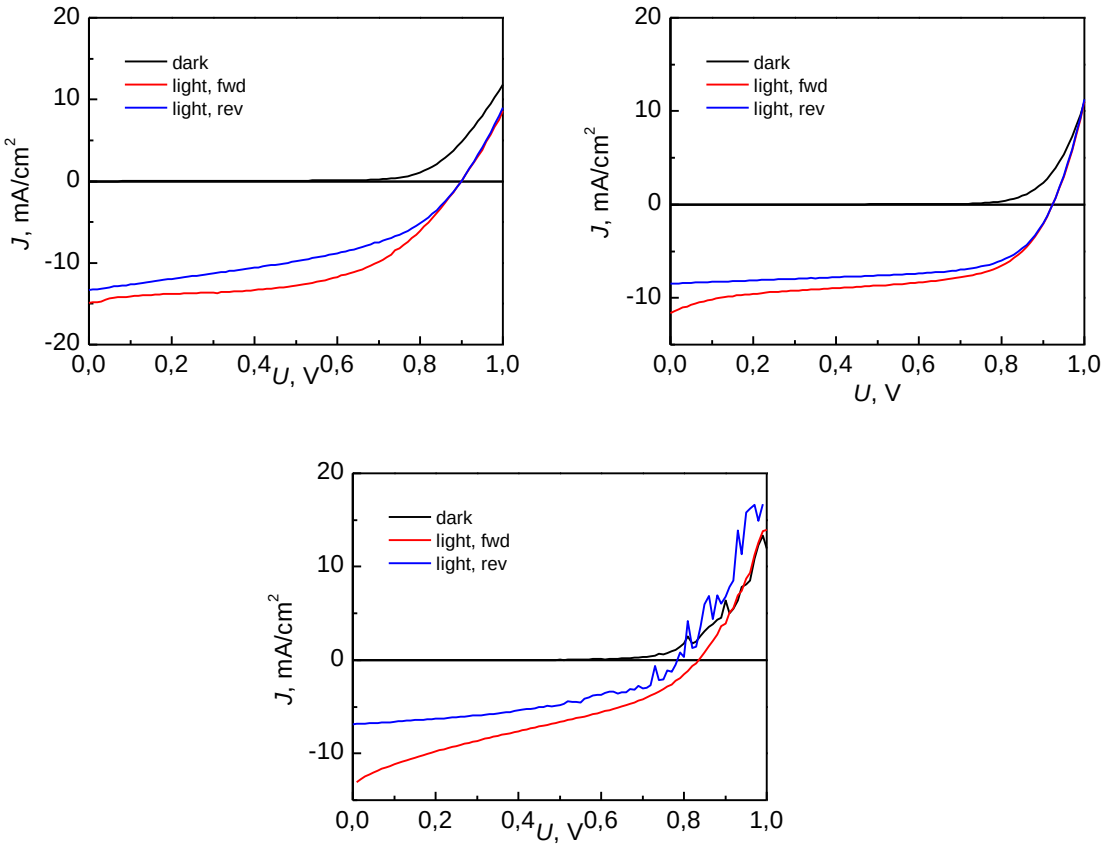

Figure 29. *J-V curves of the solar cells with 190 nm (top left), 300 nm (top right, and 400 nm (bottom) thick mesoporous layers.*

The photovoltaic parameters for the all thickness series are listed in Table 6. The results show the best efficiency with the 190 nm thick mesoporous layer, and the worst with the 400 nm thick layer. The thinnest tested layer performed the best. The efficiencies and currents are lower than in previous experiments, but the open circuit voltage 0.92 V is the highest achieved in this work. The unevenness between the results between different series is expected. The low efficiencies in this series can be explained by the reproducibility issues of perovskite.

Table 6. *Spin-coating of the solar cells with 1) 190 nm, 2), 300 nm, and 3) 400 nm thick mesoporous layers.*

Sample	Thickness of mesoporous TiO_2 (nm)	Scan direction	η (%)	*FF* (%)	J_{SC} (mA/cm2)	V_{OC} (V)
1	190	forward	7.13	53.71	14.91	0.89
1	190	reverse	5.35	45.05	13.34	0.89
2	300	forward	5.53	51.87	11.60	0.92
2	300	reverse	4.98	63.68	8.49	0.92
3	400	forward	3.32	30.98	13.06	0.82
3	400	reverse	2.54	46.63	6.88	0.79

The results for the mesoporous titania layer optimization show that 190 nm thick layer produces the best-performing perovskite solar cells. Optimization could be investigated further by testing even thinner mesoporous layers or even by omitting the mesoporous layer completely.

4.3 Characterization of perovskite and hole transport layer

The perovskite formation on top of mesoporous titania in the cleanroom conditions and its degradation are an interest of this Thesis. This required the investigation of the lead iodide film, to judge if there is unreacted lead iodide left. The analysis methods were absorption and reflectance spectroscopies, as well as scanning electron microscopy. Also the hole transport layer was investigated with these methods as a curiosity.

The absorption spectra (Figure 30) were recorded from the sintered titania layers, lead iodide film, and perovskite layer. The lead iodide film has a broad absorption band at the lower wavelength area of the spectrum. The perovskite layer absorbs at some degree throughout the entire spectrum. Compared to the absorption spectrum of lead iodide, perovskite has an additional absorption band between 500–700 nm. The absorbance level of the perovskite layer is above 2 almost in the whole recorded wavelength range. According to Equation (3) if the absorbance is close to 2 the transmittance is 0.10, which means that the part of passing light is very low. Since the prepared perovskite layers are very thick, and thus almost non-transparent, as discussed above, the reliability of the direct absorbance measurement suffers, because the instrument collects also the light, which is reflected or scattered from the film, and interprets it as absorbance. Reflectance spectra with integrating sphere technique are recorded to complement the absorbance measurements.

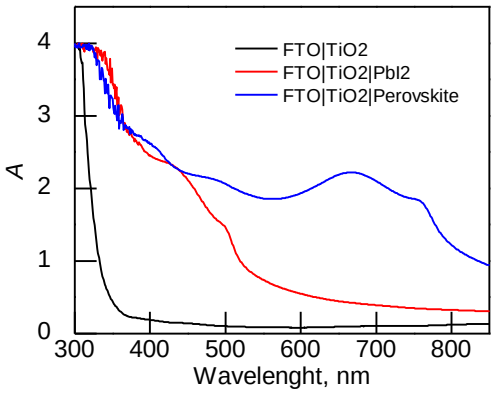

Figure 30. *Absoption spectra of titania, lead iodide and perovskite layers on top of FTO substrate.*

Figure 31 depicts the absorbance and reflectance of the lead iodide film on top of titania and FTO substrate. In general, the reflectance spectrum can provide some information about the shape of the absorption spectrum. In some measurements the two spectra are mirror images of each other. Scattering increases at lower wavelengths, which explains the steady increase of reflectance from 700 nm to 400 nm. The reflectance drops around 500 nm, which points out that there is sharp absorption band edge. This edge is not as sharp in the absorption spectrum but the band position is the same.

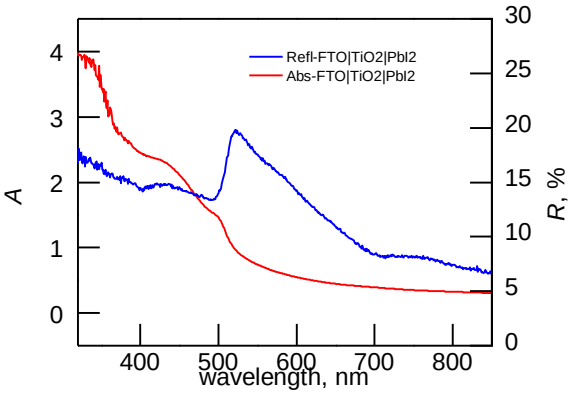

Figure 31. *Absorption and reflectance spectra of lead iodide on top of titania and FTO substrate.*

Figure 32 shows the absorption and reflectance spectra recorded from the perovskite layer on top of titania and FTO substrate. The two spectra correspond quite well to each other. The shape of the absorption spectrum corresponds to the real shape quite well in the direct absorption measurements. The absorption band edge is not sharp in the absorption spectrum due to scattering. The reflectance spectrum indicates that perovskite starts absorbing below 800 nm and the absorption band edge is very sharp.

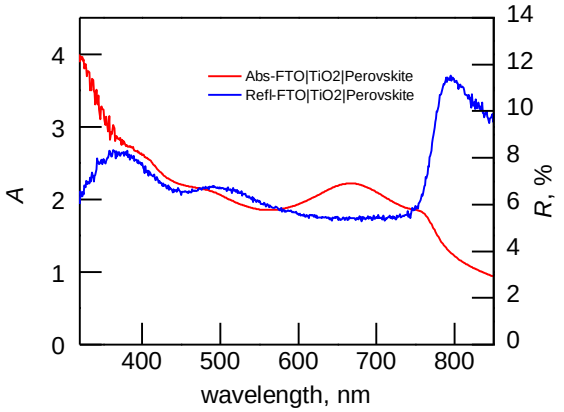

Figure 32. *Absorption and reflectance spectra of perovskite on top of titania and FTO substrate.*

The recorded reflectance after each layer is shown in Figure 33. The reflectance levels are not comparable to each other because there is deviation in the area of the samples. The spectra are recorded only for comparison of their shapes. The titania layer on top of FTO is highly transmitting and shows very little reflectance. The hole transport layer and perovskite have quite similar reflectance spectra.

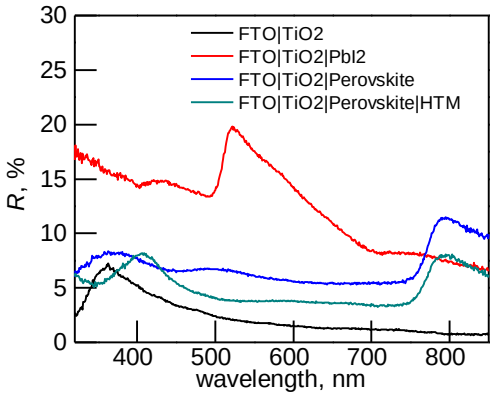

Figure 33. *Reflectance spectra after each solution-processed layer in the solar cells.*

Figure 34 presents the SEM images of top of the perovskite layer. The images were recorded after storing the sample in vacuum overnight. The images show that perovskite crystals have a cuboid shape. The coverage of the titania layer is not complete even though by eye the perovskite film is smooth and covers the titania layer completely. The perovskite crystals are evenly distributed on top of the titania layer, but perovskite does not form an uniform capping layer. Compared to the SEM images in the literature (Ref. [49]) there is not seen unreacted lead iodide in Figure 34.

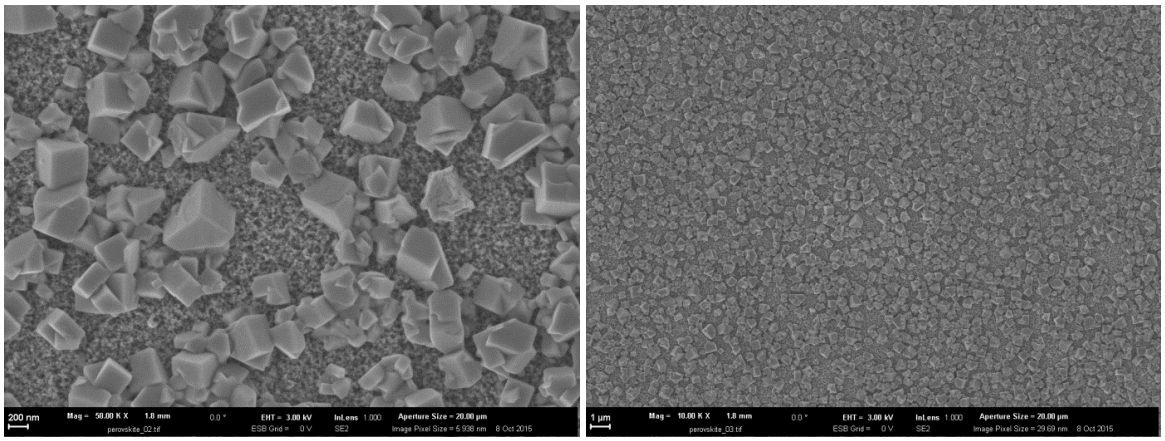

Figure 34. *SEM images of perovskite on top of mesoporous titania.*

A SEM image of the hole transport layer is shown in Figure 35. The HTM covers the bare titania layer and the perovskite layer. The perovskite morphology is still visible through the hole transport layer.

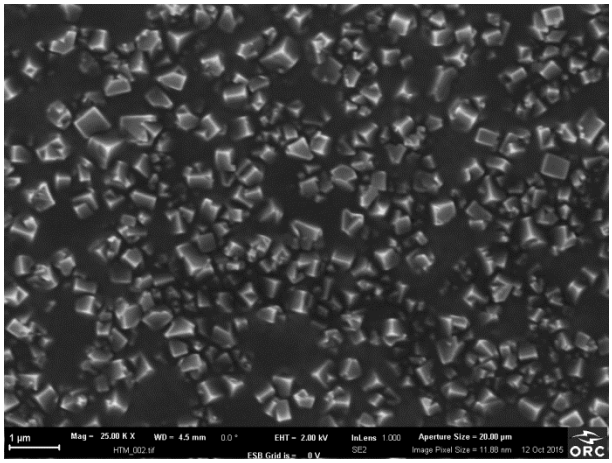

Figure 35. *SEM image of the hole transport layer from the top.*

Figure 36 represents cross-sectional SEM images of the complete solar cell structure. The layers from the bottom to top are FTO, compact titania, mesoporous titania, perovskite, HTM, and gold electrode. The images show that the HTM prevents the direct contact between perovskite and gold. It also prevents the contact between titania and gold electrode. There is not a uniform capping layer of perovskite. The height of the perovskite crystals is between 200 and 300 nm. Together the perovskite and HTM are approximately 300 nm thick.

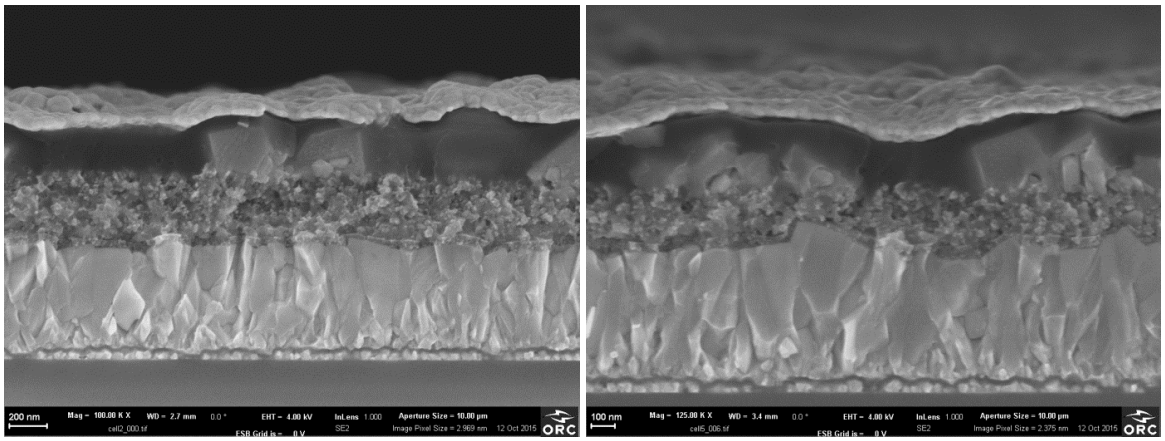

Figure 36. *Cross-sectional SEM images of the complete mesoscopic perovskite solar cell structure.*

Based on the characterization of the perovskite layer it is difficult to draw firm conclusions whether there is unreacted lead iodide left or not, although it is not seen in the SEM images. The coverage of the perovskite layer is not as high as desired. This might be due to fabrication and storing in the ambient air in the cleanroom.

5. CONCLUSIONS

This Thesis was carried out in 2015 at the Supramolecular Photochemistry Research Group, Tampere University of Technology. Perovskite solar cells have been a new research topic of the group since 2014.

The work focused on compact and mesoporous titania layers as anode materials in mesoscopic perovskite solar cells. This was the first time that group fabricated titania anodes. In fact, prior to this Thesis, the perovskite solar cells had been constructed on commercially available substrates coated with titania layers. In the present work a special attention was paid to learn and adopt the most precise preparation and measurement methods, following to the newest protocols and guidelines published in the literature.

The compact layer optimization was conducted by testing different spin-coatable compact titania layer precursor solutions. The thickness of the compact layer was studied. Spin-coating was adopted as the compact layer deposition method because of its simplicity. The best compact layer solution was prepared from titanium isopropoxide with hydrochloric acid and anhydrous ethanol. Future work should study different fabrication techniques for the compact layer, such as atomic layer deposition and spray pyrolysis.

Spin-coating was chosen as the method for mesoporous titania layer fabrication. Two alternative methods, namely doctor-blading and screen-printing, were evaluated and subsequently ruled-out because they produce thicker films compared to those fabricated via spin-coating. The mesoporous layer optimization was carried-out by varying the concentration of the solution and the spin-coating parameters. It was found that the thinnest produced film, 190 nm thick mesoporous titania layer, led to the best performing solar cells, thus suggesting that future work should concentrate on the solar cell performance at thinner mesoporous layers. In addition to further thickness tests, different titania nanoparticles pastes should be evaluated. Moreover it might be interesting to study different nanostructures and alternative metal oxides as the anode material.

In this Thesis work, the hole transport material spiro-OMeTAD with additives was adopted in perovskite solar cells for the first time by the researchers at TUT. The HTM employment was found to be successful, though the optimization of the layer was beyond the scope of this work. The HTM layer also protected the moisture sensitive

perovskite layer in the cells, thus allowing the device operation even in ambient air with relative humidity above 40 %.

The best-performing cell achieved the efficiency of 9.55 % in the forward and 8.99 % in the reverse scans. To date, this is the highest solar cell efficiency measured by the group. These results are extremely promising considering the sub-optimal environmental conditions and the early stage of the research with this type of solar cells. The record efficiencies were achieved after one week of the cell storage in darkness. The efficiency of the devices immediately after fabrication was lower. This is an interesting phenomenon that should be studied more extensively.

This Thesis contributed significantly to perovskite solar cell research. Self-made titania anodes were successfully applied and studied in perovskite solar cells. The perovskite solar cells presented in this work have been fabricated and characterized via the most up-to-date and precise methods.

REFERENCES

[1] Boundless, Visible Light, Boundless Physics, Boundless, 21 Jul. 2015. Retrieved 24 Nov. 2015.
Available: https://www.boundless.com/physics/textbooks/boundless-physics-textbook/electromagnetic-waves-23/the-electromagnetic-spectrum-165/visible-light-595-11291/

[2] A. Hagfeldt, G. Boschloo, L. Sun, L. Kloo, H. Pettersson, Dye-sensitized solar cells, Chemical Reviews, Vol. 110, No. 11, 2010, pp. 6595-6663.

[3] Interrnational Energy Statistics, Key World Energy Statistics 2014, Available: http://www.iea.org/publications/freepublications/publication/keyworld2014.pdf.

[4] C.-Y. Hsu, Y.-C. Chen, R. Yeh-Yung Lin, K.-C. Hob, J.T. Lin, Solid-state dye-sensitized solar cells based on spirofluorene (spiro-OMeTAD) and arylamines as hole transporting materials, Phys. Chem. Chem. Phys., Vol. 14, 2012, pp. 14099-14109.

[5] M.A. Green, K. Emery, Y. Hishikawa, W. Warta, E.D. Dunlop, Solar cell efficiency tables (version 46), Progress in Photovoltaics: Research and Applications, Vol. 23, No. 7, 2015, pp. 805-812.

[6] S.D. Stranks, H.J. Snaith, Metal-halide perovskites for photovoltaic and light-emitting devices, Nature Nanotechnology, Vol. 10, 2015, pp. 391–402.

[7] S. Shi, Y. Li, X. Li, H. Wang, Advancements in all-solid-state hybrid solar cells based on organometal halide perovskites, Mater. Horiz., Vol. 2, 2015, 378-405.

[8] B.V. Lotsch, New Light on an Old Story: Perovskites Go Solar, Angewandte Chemie International Edition, Vol. 53, No. 3, 2014, pp. 635-637.

[9] M.A. Green, A. Ho-Baillie, H.J. Snaith, The emergence of perovskite solar cells, Nature Photonics, Vol. 8, 2014, pp. 506–514.

[10] E. Hecht, Optics, 4th ed., Addison Wesley, 2002, 67 p.

[11] Gigahertz-Optik, Inc., Reflection, Transmission, and Absorption, 2015. Available: http://light-measurement.com/reflection-absorption/

[12] T. Engel, Quantum Chemistry & Spectroscopy, 2nd ed, Pearson, 2010, pp. 6, 67, 306.

[13] B. Valeur, Molecular Fluorescence: Principles and Applications, WILEY-VCH Verlag GmbH, 2002, pp. 20-91.

[14] N.V. Tkachenko, Optical Spectroscopy: Methods and Instrumentations, Elsevier, 2006, 9 p.

[15] S. Kazim, M.K. Nazeeruddin, M. Grätzel, S. Ahmad, Perovskite as Light Harvester: A Game Changer in Photovoltaics, Angewandte Chemie International Edition, Vol. 53, No. 11, 2014, pp. 2812-2824.

[16] Z. Yang, W. Zhang, Organolead halide perovskite: A rising player in high-efficiency solar cells, Chinese Journal of Catalysis, Vol. 35, No. 7, 2014, pp. 983-988.

[17] Y.-C. Hsiao, T. Wu, M. Li, Q. Liu, W. Qina, B. Hu, Fundamental physics behind high-efficiency organo-metal halide perovskite solar cells, J. Mater. Chem. A, Vol. 3, 2015, pp. 15372-15385.

[18] P. Gao, M. Grätzel, M.K. Nazeeruddin, Organohalide lead perovskites for photovoltaic applications, Energy Environ. Sci., Vol. 7 2014, pp. 2448-2463.

[19] G. Niu, X. Guo, L. Wang, Review of recent progress in chemical stability of perovskite solar cells, J. Mater. Chem. A, Vol. 3 2015, pp.8970-8980.

[20] B. Wang, X. Xiao, T. Chen, Perovskite photovoltaics: a high-efficiency newcomer to the solar cell family, Nanoscale, Vol. 6, 2014, pp. 12287-12297.

[21] X. Fan, M. Zhang, X. Wang, F. Yangb, X. Meng, Recent progress in organic-inorganic hybrid solar cells, J. Mater. Chem. A, Vol. 1, 2013, 8694-8709.

[22] K.D.G. Imalka Jayawardena, L.J. Rozanski, C.A. Mills, M.J. Beliatis, N.A. Nismya, S. R. P. Silva, 'Inorganics-in-Organics': recent developments and outlook for 4G polymer solar cells, Nanoscale, Vol. 5, 2013, 8411-8427.

[23] M. Wright, A. Uddin, Organic—inorganic hybrid solar cells: A comparative review, Solar Energy Materials and Solar Cells, Vol. 107, 2012, pp. 87-111.

[24] J. Yan, B.R. Saunders, Third-generation solar cells: a review and comparison of polymer:fullerene, hybrid polymer and perovskite solar cells, RSC Adv., Vol. 4, 2014, 43286-43314.

[25] N. Park, Perovskite solar cells: an emerging photovoltaic technology, Materials Today, Vol. 18, No. 2, 2015, pp. 65-72.

[26] P. Docampo, S. Guldin, T. Leijtens, N.K. Noel, U. Steiner, H.J. Snaith, Lessons Learned: From Dye-Sensitized Solar Cells to All-Solid-State Hybrid Devices, Advanced Materials, Vol. 26, No. 24, 2014, pp. 4013-4030.

[27] S. Gamliel, L. Etgar, Organo-metal perovskite based solar cells: sensitized versus planar architecture, RSC Adv., Vol. 4, 2014, pp.29012-29021.

[28] T. C. Sum, N. Mathews, Advancements in perovskite solar cells: photophysics behind the photovoltaics, Energy Environ. Sci., Vol. 7, 2014, pp. 2518-2534.

[29] N-G. Park, Organometal Perovskite Light Absorbers Toward a 20% Efficiency Low-Cost Solid-State Mesoscopic Solar Cell, J. Phys. Chem. Lett., Vol. 4, No. 15, 2013, 4 (15), pp 2423–2429.

[30] Y. Wu, X. Yang, H. Chen, K. Zhang, C. Qin, J. Liu, W. Peng, A. Islam, E. Bi, F. Ye, Highly compact TiO 2 layer for efficient hole-blocking in perovskite solar cells, Applied Physics Express, Vol. 7, No. 5, 2014, pp. 05230-1–4.

[31] X. Wang, Y. Fang, L. He, Q. Wang, T. Wu, Influence of compact TiO2 layer on the photovoltaic characteristics of the organometal halide perovskite-based solar cells, Mater. Sci. in Semic. Proc., Vol. 27, 2014, pp. 569-576.

[32] D.A. H. Hanaor, C. C. Sorrell, Review of the anatase to rutile phase transformation, J. Mater. Sci., Vol. 46, 2011, pp. 855–874.

[33] Titanium Dioxide (TiO_2) Photocatalysis in Concrete. Available: https://pavemaintenance.wikispaces.com/TiO2+Photocatalys+-+Shannon.

[34] Y. Zhang, W. Liu, F. Tan, Y. Gu, The essential role of the poly(3-hexylthiophene) hole transport layer in perovskite solar cells, Journal of Power Sources, Vol. 274, No. 0, 2015, pp. 1224-1230.

[35] P. Gratia, A. Magomedov, T. Malinauskas, M. Daskeviciene, A. Abate, S. Ahmad, M. Grätzel, V. Getautis, M.K. Nazeeruddin, A Methoxydiphenylamine-Substituted Carbazole Twin Derivative: An Efficient Hole-Transporting Material for Perovskite Solar CellsAngew. Chem. Int. Ed., Vol. 54, No. 39, 2015, pp. 11409-11413.

[36] J. Burschka, A. Dualeh, F. Kessler, E. Baranoff, N. –L. Cevey-Ha, C. Yi, M. K. Nazeeruddin, and M. Grätzel, Tris(2-(1H-pyrazol-1-yl)pyridine)cobalt(III) as p-Type Dopant for Organic Semiconductors and Its Application in Highly Efficient Solid-State Dye-Sensitized Solar Cells, J. Am. Chem. Soc., Vol. 133, No. 45, 2011, pp. 18042–18045.

[37] J. Burschka, N. Pellet, S.-J. Moon, R. Humphry-Baker, P. Gao, M.K. Nazeeruddin, M. Grätzel ,Sequential deposition as a route to high-performance perovskite-sensitized solar cells, Nature, Vol. 499,2013, pp.316–319.

[38] A. Abate, T. Leijtens, S. Pathak , J. Teuscher, R. Avolio, M. E. Errico, J. Kirkpatrik, J.M. Ball, P. Docampo, I. McPherson, H.J. Snaith, Lithium salts as "redox active" p-type dopants for organic semiconductors and their impact in solid-state dye-sensitized solar cells, Phys. Chem. Chem. Phys., Vol. 15, 2013, 2572-2579.

[39] H.S. Jung, N. Park, Perovskite Solar Cells: From Materials to Devices, Small, Vol. 11, No. 1, 2015, pp. 10-25.

[40] M. Ye, X. Wen, M. Wang, J. Iocozzia, N. Zhang, C. Lin, Z. Lin, Recent advances in dye-sensitized solar cells: from photoanodes, sensitizers and electrolytes to counter electrodes, Materials Today, Vol. 18, No. 3, 2015, pp. 155-162.

[41] X. Yang, M. Yanagida, L. Han, Reliable evaluation of dye-sensitized solar cells, Energy and Environ. Sci., Vol. 6, No. 1, 2013, pp. 54-66.

[42] RREDC, Reference Solar Spectral Irradiance: ASTM G-173. Available: http://rredc.nrel.gov/solar/spectra/am1.5/ASTMG173/ASTMG173.html

[43] J.A. Christians, J.S. Manser, P.V. Kamat, Best Practices in Perovskite Solar Cell Efficiency Measurements. Avoiding the Error of Making Bad Cells Look Good, J. Phys. Chem. Lett., Vol. 6, No. 5, 2015, pp 852–857.

[44] H.J. Snaith, How should you measure your excitonic solar cells?, Energy Environ. Sci., Vol. 5, 2012, pp.6513-6520.

[45] Shimadzu, Diffuse Reflectance Measurement. Available: http://www.shimadzu.com/an/spectro/uv/accessory/solidsample/solid.html.

[46] N.-G. Park, Organometal Perovskite Light Absorbers Toward a 20% Efficiency Low-Cost Solid-State Mesoscopic Solar Cell, J. Phys. Chem. Lett., Vo.l. 15, No. 4, 2013, pp. 2423–2429.

[47] H.-S. Kim, C.-R. Lee, J.-H. Im, K.-B. Lee, T. Moehl, A. Marchioro, S.-J. Moon, R. Humphry-Baker, J.-H. Yum, J. E. Moser, M. Grätzel, N.-G. Park, Lead Iodide Perovskite Sensitized All-Solid-State Submicron Thin Film Mesoscopic Solar Cell with Efficiency Exceeding 9 %, Scientific Reports 2, No. 591, 2012.

[48] S. Pathak, A. Sepe, A. Sadhanala, F. Deschler, A. Haghighirad, N. Sakai, K. C. Goedel, S. D. Stranks, N. Noel, M. Price, S. Hüttner, N.A. Hawkins, R.H. Friend, U. Steiner, H.J. Snaith, Atmospheric Influence upon Crystallization and Electronic Disorder and Its Impact on the Photophysical Properties of Organic–Inorganic Perovskite Solar Cells, ACS Nano, Vol.6, No. 3, 2015, pp. 2311–2320.

[49] Q. Chen, H. Zhou, Z. Hong, S. Luo, H.-S. Duan, H.-H. Wang, Y. Liu, G. Li, Y. Yang, Planar Heterojunction Perovskite Solar Cells via Vapor-Assisted Solution Process, J. Am. Chem. Soc., Vol. 136, No. 2, 2014, pp 622–625.